International Congress of Parkinson's Disease and Movement Disorders®

mdscongress.org

Late-Breaking Abstracts

International Parkinson and Movement Disorder Society

Philadelphia, PA, USA

September 27-October 1, 2024

International Congress of Parkinson's Disease and Movement Disorders®

2024 Late-Breaking Abstracts

LBA-1: Natural progression of multiple system atrophy in a Chinese population

H. Shang; P. Chan; Q. Zhou; A. Rieckmann; A. Bidani; D. Oudin Åström (Beijing, China)

LBA-2: Quantitative Measurements of α-Synuclein Seeds in Cerebrospinal Fluid Inform Diagnosis and Staging of Synucleinopathies

O. El-Agnaf; I. Abdi; I. Sudhakaran; S. Ghanem; V. Constantinides; E. Kapaki; W. van de Berg; D. Erskine; B. Mollenhauer; L. Parkkinen; M. Schlossmacher (Ar Rayyan, Qatar)

LBA-3: A Novel Continuous Quantitative Measurement of Cutaneous Phosphorylated Alpha-Synuclein in PD, MSA and DLB

B. Bellaire; T. Levine; R. Freeman (Boston, MA, USA)

LBA-4: Anti-tetanus vaccination is associated with reduced occurrence and slower progression of Parkinson's disease

E. Magen; E. Ruppin; E. Merzon; S. Vinker; N. Giladi (Jerusalem, Isreal)

LBA-5: Liquid Chromatograph Mass Spectrometer and mendelian randomization based on serum metabolomics biomarker discovery of Parkinson's disease

L. Zhuang; X. Liu (Philadelphia, PA, USA)

LBA-6: Frequency-selective suppression of essential tremor via transcutaneous spinal cord electrical stimulation

A. Pascual-Valdunciel; J. Ibanez; L. Rocchi; J. Song; J. Rothwell; K. P. Bhatia; D. Farina; A. Latorre (London, United Kingdom)

LBA-7: Diving into Health: Revolutionizing Parkinson's Disease Rehabilitation with Aquatic HIIT

F. Nazemi; A. Chitsaz; N. Salimian; A. Alipur Shehni; S. Ahmadi (Isfahan, Iran)

LBA-8: 3 Classification of alpha synuclein aggregation in the brain by neural derived EV-bound biomarkers in blood in Parkinson's Disease

G. Ho; R. Samat; P. Maimonis; M. Marken; M. Cantillon

LBA-9: First in Human Administration of an Autologous Investigational Cell Therapy for Parkinson Disease Using an Intraoperative MRI-guided Posterior Approach

C. Christine; N. Phielipp; M. Houser; S. Sherman; E. Wirth III (San Diego, CA, USA)

LBA-10: The novel glucocerebrosidase chaperone GT-02287 in development for GBA-PD is safe and well tolerated in healthy volunteers at oral doses that produce plasma exposures in the projected therapeutic range

M. De Sciscio; M. Bosetti; P. Martin; S. Cano; B. Guzman; A. Marcinowicz; A. Rozwadowsk; A. Schreiner; N.Dzamko; J. Taylor; T. Ignoni; J. Hannestad (Bethesda, MD, USA)

LBA-11: A Phase 3, Randomized, Assessor-blind, Active-Controlled Study of Pimavanserin in Comparison with Quetiapine in Parkinson's Disease Psychosis

B. Kathiriya; Y. Patidar; V. Patel,; A. Singhal; B. Patel; S. Choudhury; R. Varadarajulu; A. Pattojoshi; B. Solanki; A. Sharma; A. Pande; K. Parmar; S. Jayalekshmi; R. Mridula; N. Sundarachary; P. Walzade; S. Ramteke; D. Kumar; P. Kumar; D. Sonawane; P. Devkare; M. Rajurkar; D. Patil; P. Ghadge; S. Mehta (Mumbai, India)

LBA-12: Efficacy and Safety of Tavapadon, an Orally Administered, Once-Daily, Selective D1/D5 Partial Dopamine Agonist, Adjunctive to Levodopa for Treatment of Parkinson's Disease With Motor Fluctuations

S. Isaacson; R. Last Name; P. Agarwal; W. Ondo; A. Park; L. Elmer; D. Kremens; M. Leoni; S. Duvvuri; C. Combs; E. Koenig; I. Chang; G. Pastino; S. Tringali; N. Golonski; R. Sanchez (Cary, NC, USA)

LBA-13: AI-based 3D anthropometric modeling for automated assessment and grading of dystonia patients

K. Dev Nayar; N. Ganza; S. Begalan; C. Go; A. Hunt; P. Acuna; N. Sharma (Boston, MA, USA)

LBA-14: The ki: SB-M Intelligibility Score — An Automatic Measure for Intelligibility in Motor Speech Disorders

F. Dörr; L. Schwed; N. Linz; A. König; T. Thies; M. Barbe; J. Orozco-Arroyave; J. Rusz (Saarbrucken, Germany)

LBA-15: A Neuroimaging-Based Diagnostic Model of Parkinson's Disease Using Bootstrap Aggregating Deep Neural Network Classifiers

K. Van Hedger; N. Rothery; K. Seergobin; M. Elganga; D. Michels; A. Omar; H. Ganjavi; M. Khalil; A. Sarkar; P. MacDonald (London, ON, Canada)

LBA-16: Deep Brain Stimulation does not modify the cognitive trajectory of GBA-PD: a longitudinal study of the Italian PARKNET cohort

C. Artusi; R. Cilia; G. Giannini; G. Cuconato; C. Pasquini; A. Albanese; N. Andreasi; A. Antonini; L. Avanzino; A. Bentivoglio; F. Bove; M. Bozzali; G. Calandra-Buonaura; V. Carelli; F. Cavallieri; A. Cocco; F. Cogiamanian; F. Colucci; P. Cortelli; F. Di Biasio; A. Di Fonzo; V. D'Onofrio; R. Eleopra; A. Elia; V. Fioravanti; A. Guerra; C. Ledda; M. Liccari; C. Longo; L. Lopiano; M. Malaguti; F. Mameli; S. Marino; R. Minardi; E. Monfrini; C. Pacchetti; C. Piano; V. Rispoli; M. Rizzone; L. Romito; L. Sambati; M. Sensi; C. Sorbera; F. Spagnolo; C. Tassorelli; F. Valentino; F. Valzania; R. Zangaglia; M. Zibetti; The ParkNet Study Group; E. Valente (Italy)

LBA-17: PSMF1 variants cause a phenotypic spectrum from early-onset Parkinson's disease to perinatal lethality by disrupting mitochondrial pathways

C. Tesson; P. Angelova; A. Salazar-Villacorta; J. Rodriguez; A. Scardamaglia; B. Chung; M. Jaconelli; B. Vona; N. Esteras; A. Kwong; T. Courtin; R. Maroofian; S. Alavi; R. Nirujogi; M. Severino; P. Lewis; S. Efthymiou; B. O'Callaghan; R. Buchert; L. Sofan; P. Lis; C. Pinon; G. Breedveld; M. Chui; D. Murphy; V. Pitz; M. Makarious; M. Cassar; B. Hassan; S. Iftikhar; C. Rocca; P. Bauer; M. Tinazzi; M. Svetel; B. Samanci; H. Hanağası; B. Bilgiç; J. Obeso; M. Kurtis; G. Cogan; A. Başak; G. Kiziltan; T. Gül; G. Yalçın-Cakmakli; B. Elibol; N. Barišić; E. Ng; S. Fan; T. Hershkovitz; K. Weiss; J. Raza Alvi; T. Sultan; I. Azmi Alkhawaja; T. Froukh; H. Abdollah E Alrukban; C. Fauth; U. Schatz; T. Zöggeler; M. Zech; K. Stals; V. Varghese; S. Gandhi; C. Blauwendraat; J. Hardy; S. Lesage; V. Bonifati; T. Haack; A. Bertoli-Avella; R. Steinfeld; D. Alessi; H. Steller; A. Brice; A. Abramov; K. Bhatia; H. Houlden (London, United Kingdom)

LBA-18: Preliminary Efficacy and Safety of ATH434 in Multiple System Atrophy

A. Brown; A. Wynn; C. Wong; K. Kmiecik; P. Trujillo; M. Bradbury; D. Stamler (Nashville, TN, USA)

LBA-19: Results of ALLEVIA 1 (NOE-TTS-211; EudraCT 2021-004424-15; ANZCTR ACTRN12621000319875), a Phase 2a study exploring safety and tolerability of NOE-105 in patients with Tourette Syndrome

G. Garibaldi; R. Lasser; K. Mueller-Vahl (Hannover, Germany)

LBA-20: Nonhuman primate efficacy and safety of snp614, a lrrk2 antisense oligonucleotide as potential therapeutic agent for parkinson's disease

A. Zembrzycki;Y. Martens; I. Riera Tur;S. Michel; R. Klar; F. Jaschinski; G. Bu; M. Li (Rockville, MD, USA)

LBA-1: Natural progression of multiple system atrophy in a Chinese population

H. Shang; P. Chan; Q. Zhou; A. Rieckmann; A. Bidani; D. Oudin Åström (Beijing, China)

Objective: Describe the natural progression of early multiple system atrophy (MSA) in a Chinese population.

Background: Understanding disease natural history is important for the development of potential disease-modifying treatments for people with MSA. However, the early stages, when a disease-modifying treatment would be expected to be most beneficial, are not well characterized with a clear evidence gap in non-Western populations.

Method: Multicenter, observational study conducted in 8 sites across China. Eligible participants were aged 40–75 years, with possible or probable MSA of the parkinsonian (MSA-P) or cerebellar (MSA-C) subtype, anticipated survival of at least 3 years, UMSARS-Chinese version Part I score of ≤16 (omitting Q11 on sexual function), and a Montreal Cognitive Assessment score ≥22. Patients were followed for one year; standard of care treatments were prescribed according to routine clinical practice. Disease progression was analyzed using a linear mixed model of Total UMSARS (Part I+II) progression, including baseline, Month 6 and Month 12 data.

Results: A total of 89 participants (66.3% male, mean age 58.5 years) were enrolled; of these about half (52%) had MSA-C and 48% participants had MSA-P. The mean time since onset of motor symptoms was 2.2 years and time since MSA diagnosis was 0.4 years. The mean ± SE [95%CI] rate of Total UMSARS progression was 1.27 ± 0.13 [1.01, 1.53] points per month. Participants showed a progression of 0.64 ± 0.06 [0.51, 0.76] points/month on UMSARS Part I and 0.62 ± 0.07 [0.47, 0.77] points/month on UMSARS Part II. There were no significant differences in the rates of progression between patients with MSA-P and MSA-C ($p>0.05$).

This is the first multicenter natural history study of MSA progression conducted in China. While prior studies have indicated a predominance of MSA-C in Asian populations, we found a more even split of MSA-C and MSA-P subtypes. On average, patients waited >1.5 years from onset of motor symptoms to diagnosis. In this early population, patients showed an average progression of rates of >15 Total UMSARS points/year; rates of progression were similar between the two subtypes and were in alignment with previous studies that assessed disease progression using UMSARS in Western populations.

LBA-2: Quantitative Measurements of α-Synuclein Seeds in Cerebrospinal Fluid Inform Diagnosis and Staging of Synucleinopathies

O. El-Agnaf; I. Abdi; I. Sudhakaran; S. Ghanem; V. Constantinides; E. Kapaki; W. van de Berg; D. Erskine; B. Mollenhauer; L. Parkkinen; M. Schlossmacher (Ar Rayyan, Qatar)

Objective: The objective of our study is to develop a method for diagnosing α-synucleinopathies and assessing target engagement in trials.

Background: Diagnosing α-synucleinopathies and assessing target engagement in trials is hindered by the absence of reliable biomarkers reflecting disease traits, states, rates, and fates. The need for

innovative approaches to biomarker discovery in synucleinopathies has become evident due to the limitations of existing techniques and in failures of recent trials.

Method: Introducing a first-in-kind diagnostic assay, named Seeding Amplification ImmunoAssay (SAIA), we present a quantitative, highly sensitive, and disease-specific method. This study showcases a comprehensive range of cohorts, including 37 brain homogenates and 585 cerebrospinal fluid (CSF) samples covering diverse synucleinopathies, non-synucleinopathies, prodromal rapid eye movement sleep behavior disorder (RBD) cases, LRRK2 mutation carriers at risk for Parkinson's disease (PD), and controls.

Results: SAIA achieved remarkable amplification and detection of disease-related α-synuclein (α-syn) seeds within brain homogenates diluted up to 6,400-fold and quantified even minute quantities of preformed α-syn fibrils at a level of 0.5 attograms. Demonstrating high diagnostic efficacy, SAIA distinguished synucleinopathies (PD, multiple system atrophy, and dementia with Lewy bodies) from non-synucleinopathies and controls with sensitivities and specificities ranging between 80-100%, reflected by area under the curve values exceeding 0.9. Importantly, the assay revealed a positive correlation between CSF α-syn seeds and disease severity, as measured by Unified Parkinson's Disease Rating Scale scores in PD patients. SAIA also accurately identified 24/24 (100%) iRBD cases, considered a prodromal state of PD, with 100% sensitivity and 80% specificity.

The SAIA represents a significant advancement in synucleinopathy research, bringing together diagnostic and quantification capabilities in an easily accessible format that is highly transferable into the clinical setting. The assay's relevance to early diagnosis, disease monitoring, and therapeutic trials has the potential to fill an urgent need. Further validation and expansion to less invasive biofluid samples are recommended for broader clinical utility.

LBA-3: A Novel Continuous Quantitative Measurement of Cutaneous Phosphorylated Alpha-Synuclein in PD, MSA and DLB

B. Bellaire; T. Levine; R. Freeman (Boston, MA, USA)

Objective: To develop a novel, continuous, quantitative method for analysis of cutaneous phosphorylated alpha-synuclein (P-SYN).

Background: Recent diagnostic advances to synucleinopathies such as Parkinson’s disease (PD), dementia with Lewy bodies (DLB) and multiple system atrophy (MSA) include seed amplification and skin immunofluorescent immunostaining of P-SYN. However, there is an ongoing need for an objective, continuous, quantitative measure of P-SYN deposition to monitor disease progression and the response to disease modifying interventions.

Method: We developed a digital pathology detection tool (NerValence, CND Life Sciences) to quantify misfolded proteins within cutaneous axons. We studied 20 patients each with PD, MSA and DLB and 20 healthy controls. All participants had skin biopsies at the distal leg, distal thigh and posterior cervical region with immunostaining for P-SYN and protein gene product 9.5. All tissue sections underwent confocal slide scanning and artificial intelligence driven quantitation of nerve fibers and intra-axonal P-SYN.

Results: The age was 69.3±7.1 years (PD), 74.3±7.1 years (DLB), 64.2±7.4 years (MSA) and 65.5±7.8 years (controls). The MDS-UPDRS score was 52±16 (PD), 59±18 (DLB), 85±34 (MSA) and 1.9±2.7 (controls). The MoCA was 25.3±1.9 (PD), 15.8±6.9 (DLB), 24.7±2.8 (MSA) and 28.1±1.5 (controls). The deposition of P-SYN (µm2 of P-SYN per mm2 of tissue analyzed) was 2.7±0.9 (PD), 10.1±3.2 (DLB), 12.1±3.8 (MSA), and 0±0 (controls) (, P<0.001, ANOVA. There was a strong proximal>distal P-SYN deposition gradient in PD, more modest gradient in DLB, with no gradient seen in MSA. In PD, P-SYN deposition occurred in nerve bundles and blood vessels. In DLB, the PSYN deposition occurred in nerve bundles, blood vessels, sweat glands and pilomotor muscles. In MSA, P-SYN deposition occurred in nerve bundles and the subepidermal plexus.

Digital pathologic detection of synuclein protein provides a novel, continuous, quantitative measure of P-SYN deposition. Overall topographic and regional distribution patterns of P-SYN deposition may provide the basis for differentiation among the synucleinopathies. Follow- up data are required to quantify P-SYN deposition over time.

LBA-4: Anti-tetanus vaccination is associated with reduced occurrence and slower progression of Parkinson's disease

E. Magen; E. Ruppin; E. Merzon; S. Vinker; N. Giladi (Jerusalem, Isreal)

Objective: To investigate the potential protective effect of vaccination and antimicriobial medications that could affect the microbiome on the occurrence and progression of Parkinson's Disease (PD) .

Background: Parkinson's Disease (PD) is a progressive neurodegenerative disorder characterized by symptoms such as resting tremor, bradykinesia, and rigidity. The etiology of PD remains unclear, and existing treatments do not stop the disease's progression. Emerging evidence suggests that organisms present in the microbiome may play a role in PD pathology.

Method: This large cohort study was performed within Leumit Health Services (LHS), a national health provider insuring over 720,000 members and maintaining comprehensive electronic health records (EHR) over the past 22 years.

The case patients comprised PD patients diagnosed between 2003 and 2023, aged between 45 and 75 at the date of first diagnosis. This age range was chosen to exclude the rare cases in very young patients (<45), where disease occurrence is heavily influenced by genetic factors, and older patients (>75), where non-specific motor symptoms make PD diagnosis less reliable. For each case individual, five controls were identified, matched based on gender, socio-economic status, and the year of initial enrollment in LHS. Controls were selected with birth dates closest to those of the PD patients, ensuring no individual duplication within the cohort, and were assigned the same index dates as their matched case individuals.

Using this cohort of 1,446 PD patients and 7,230 controls, we evaluated the effect of vaccination on PD occurrence. Additionally, we applied a machine learning algorithm to analyze the impact of vaccination and medication use on PD severity among PD patients.

Results: The findings reveal a significant reduction in PD occurrence following anti-tetanus-diphtheria vaccination. There was a time-dependent association between the time elapsed since vaccination and both the incidence and progression of PD.

Further analyses indicated that anti-tetanus vaccination and antimicrobial treatments significantly influenced disease severity in a manner characteristic of Clostridium microbial sensitivity profiles, suggesting the involvement of C. tetani in PD pathology.

This study suggests potential involvement of Clostridium tetani in the pathology of PD. Consequently, tetanus vaccination and C. tetani eradication could become promising strategies for preventing PD and decelerating its progression, pending further validation through clinical trials. This research offers new preventive and therapeutic avenues for PD, aligning with the interests and goals of MDS Members dedicated to advancing the understanding and treatment of movement disorders.

Table 1. Demographic and clinical characteristics of the study cohort at index date

		PD patients N=1446	Control N=7230	P	Odds Ratio
Gender	Female	655 (45.3 %)	3,275 (45.3 %)	1.000	1
	Male	791 (54.7 %)	3,955 (54.7 %)	1.000	1
Age (years)		65.7 ± 7.2	65.6 ± 7.3	0.537	
Age category	45-49	47 (3.25 %)	243 (3.36 %)	0.873	0.97
	50-59	247 (17.08 %)	1,249 (17.28 %)	0.879	0.99
	60-69	591 (40.87 %)	3,081 (42.61 %)	0.232	0.93
	70-	561 (38.80 %)	2,657 (36.74 %)	0.136	1.09
BMI (kg/m2)		28.3 ± 5.1	28.6 ± 5.1	0.035	
	missing	55 (3.80 %)	188 (2.60 %)		
BMI category	<18.5 Underweight	17 (1.22 %)	55 (0.78 %)	0.110	1.57
	18.5-24.9 Normal	330 (23.72 %)	1,618 (22.98 %)	0.554	1.04
	25-29.9 Overweight	581 (41.77 %)	2,951 (41.91 %)	0.929	0.99
	>=30 Obese	463 (33.29 %)	2,418 (34.34 %)	0.458	0.95
	missing	55 (3.80 %)	188 (2.60 %)	0.014	1.48
BP systolic (mmHg)		134 ± 25	133 ± 21	0.246	
	missing	4 (0.28 %)	41 (0.57 %)		
BP diastolic (mmHg)		78.2 ± 9.6	78.0 ± 9.5	0.491	
	missing	5 (0.35 %)	45 (0.62 %)		
Smoking status	Non-smoker	1,155 (79.88 %)	5,478 (75.77 %)	0.001	1.27
	Past smoker	43 (2.97 %)	275 (3.80 %)	0.145	0.78
	Smoker	132 (9.13 %)	1,051 (14.54 %)	<0.001	0.59
	missing	116 (8.02 %)	426 (5.89 %)	0.003	1.39
Socio-economic status (1-20)		9.72 ± 3.40	9.73 ± 3.40	0.948	
	missing	74 (5.12 %)	370 (5.12 %)		
eGFR MDRD (mL/min/1.73m2)		79.4 ± 20.2	80.6 ± 24.5	0.089	
	missing	132 (9.13 %)	844 (11.67 %)		
Glucose (mg/dL)		111 ± 32	109 ± 33	0.107	
	missing	127 (8.78 %)	807 (11.16 %)		
Hemoglobin A1c (%)		6.22 ± 1.10	6.22 ± 1.16	0.945	
	missing	418 (28.9 %)	2,490 (34.4 %)		
Record of prior Tetanus-Diphtheria toxoid vaccination		**22 (1.52 %)**	**216 (2.99 %)**	**0.001**	**0.50**

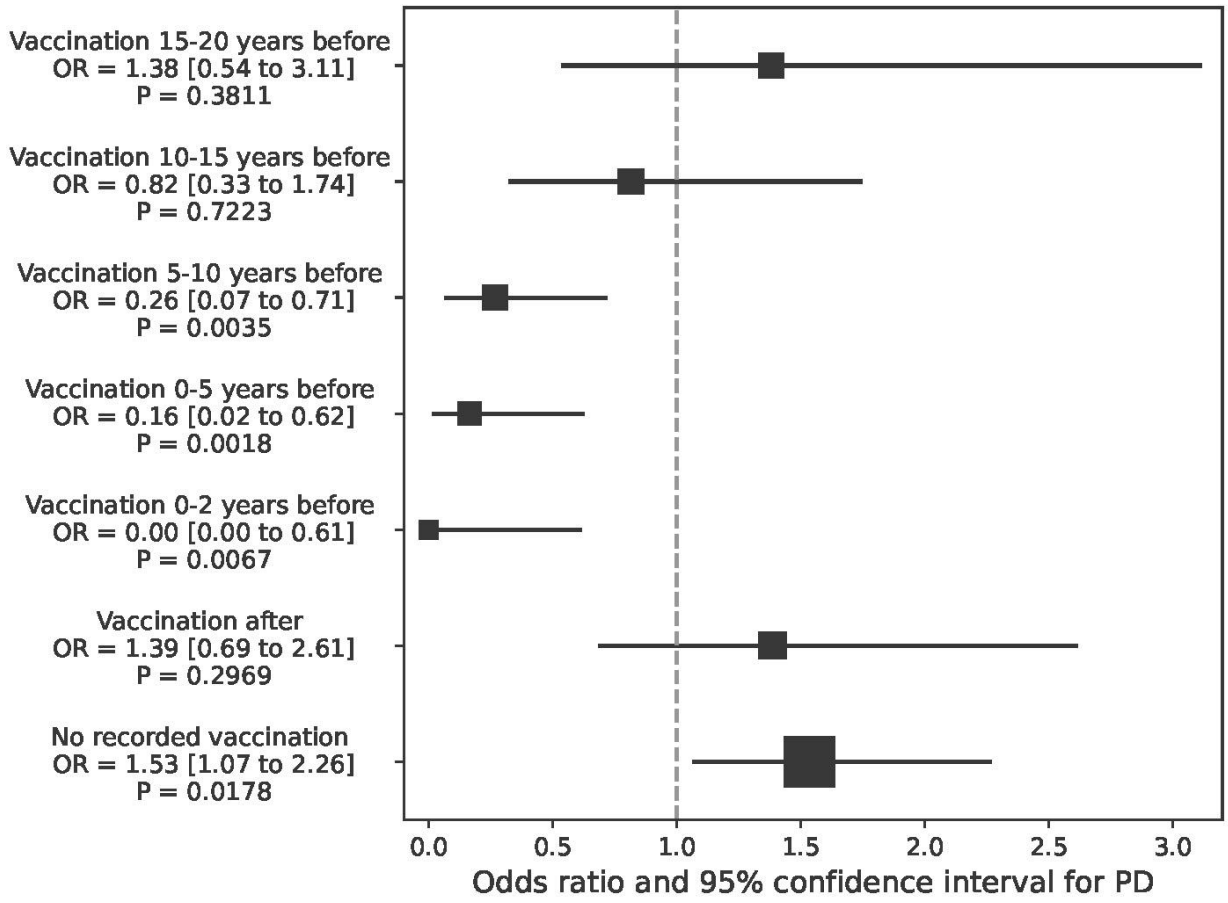
Vaccination 15-20 years before
OR = 1.38 [0.54 to 3.11]
P = 0.3811
Vaccination 10-15 years before
OR = 0.82 [0.33 to 1.74]
P = 0.7223
Vaccination 5-10 years before
OR = 0.26 [0.07 to 0.71]
P = 0.0035
Vaccination 0-5 years before
OR = 0.16 [0.02 to 0.62]
P = 0.0018
Vaccination 0-2 years before
OR = 0.00 [0.00 to 0.61]
P = 0.0067
Vaccination after
OR = 1.39 [0.69 to 2.61]
P = 0.2969
No recorded vaccination
OR = 1.53 [1.07 to 2.26]
P = 0.0178
0.0
0.5
1.0
1.5
2.0
2.5
3.0
Odds ratio and 95% confidence interval for PD

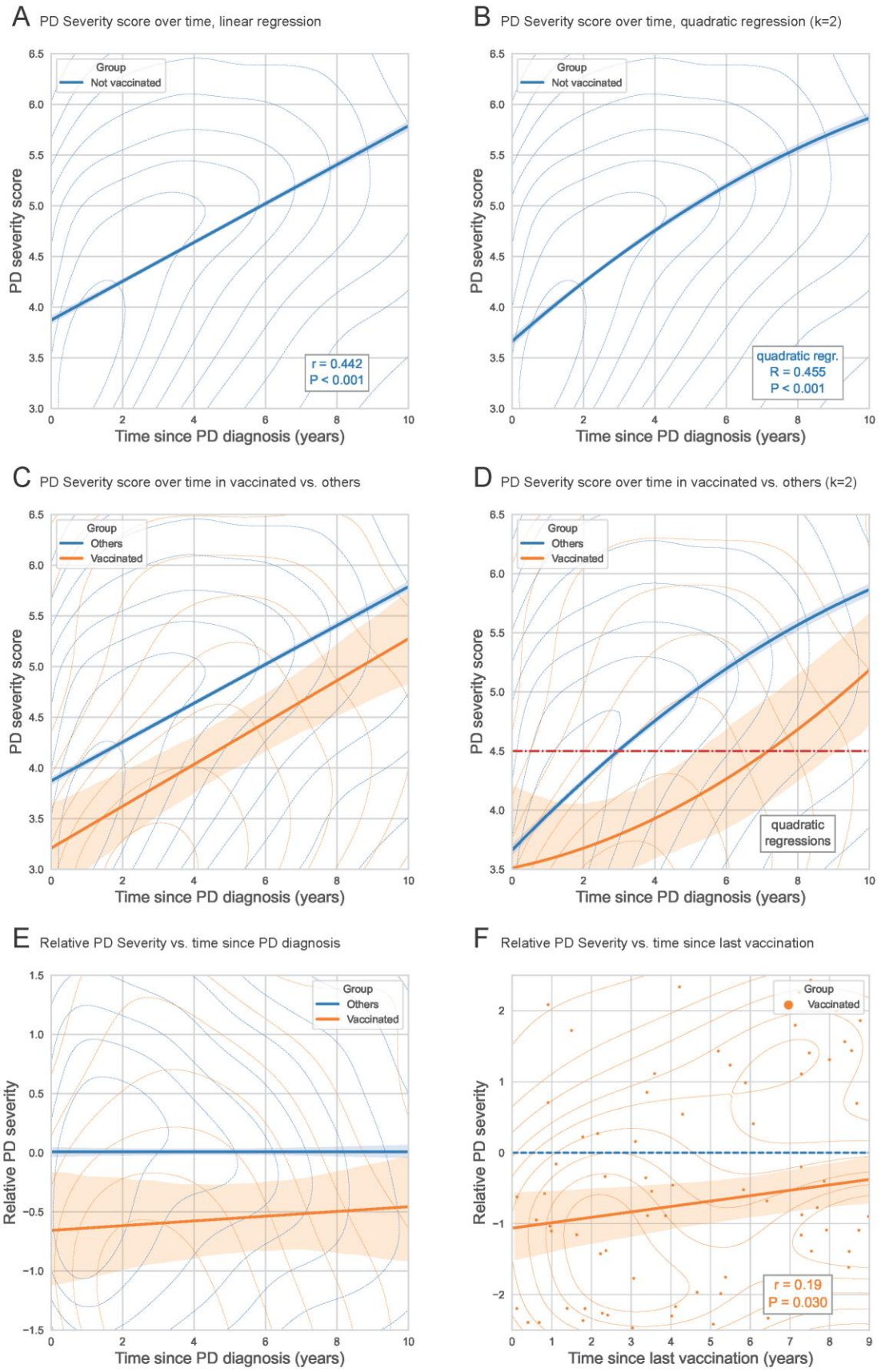
A PD Severity score over time, linear regression
Group
Not vaccinated
PD severity score
Time since PD diagnosis (years)
r = 0.442
P < 0.001
B PD Severity score over time, quadratic regression (k=2)
Group
Not vaccinated
PD severity score
Time since PD diagnosis (years)
quadratic regr.
R = 0.455
P < 0.001
C PD Severity score over time in vaccinated vs. others
Group
Others
Vaccinated
PD severity score
Time since PD diagnosis (years)
D PD Severity score over time in vaccinated vs. others (k=2)
Group
Others
Vaccinated
PD severity score
Time since PD diagnosis (years)
quadratic regressions
E Relative PD Severity vs. time since PD diagnosis
Group
Others
Vaccinated
Relative PD severity
Time since PD diagnosis (years)
F Relative PD Severity vs. time since last vaccination
Group
Vaccinated
Relative PD severity
Time since last vaccination (years)
r = 0.19
P = 0.030

LBA-5: Liquid Chromatograph Mass Spectrometer and mendelian randomization based on serum metabolomics biomarker discovery of Parkinson's disease

L. Zhuang; X. Liu (Philadelphia, PA, USA)

Objective: In this study, we combined mendelian randomization, LC-MS non targeted metabolomics, and bioinformatics analysis methods to explore changes in biochemical pathways and metabolites fingerprint related to the pathology of Parkinson's disease(PD), with the aim of finding new and easily accessible indicators of the processes underlying PD. We hypothesized that the study would offer convincingful, new, easily accessible biochemical biomarkers for promoting the diagnosis and treatment of PD. It is conducive to build a bridge between basic research and clinical translation of PD through the integration of multiple research methods

Background: Research into PD is fraught with numerous challenges, which can be broadly categorized into clinical, biological, methodological, and translational hurdles1. Currently, PD diagnosis is primarily clinical, based on symptom presentation and response to dopaminergic treatment2. The absence of reliable biomarkers for early detection and differential diagnosis from other neurodegenerative diseases is a significant barrier. Identifying biomarkers that accurately reflect disease progression is essential for monitoring the effectiveness of interventions and understanding the disease's natural history. Due to the unclear pathogenesis of PD, two challenging outcomes have emerged: 1. Lack of appropriate biomarkers leading to a higher misdiagnosis rate. 2. Lack of suitable drug treatment targets.

Over the past decades, metabolomics has emerged as a powerful tool for early diagnosis and track disease progression3. Metabolic changes often precede clinical symptoms, making metabolomic biomarkers valuable for early detection4.Metabolomics can help track disease progression by identifying biomarkers that correlate with disease severity and stage5. This is particularly important for monitoring the effectiveness of therapeutic interventions and for stratifying patients in clinical trials.

Each neurodegenerative disease exhibits a unique metabolic fingerprint1. By comparing the metabolomic profiles of healthy individuals with those affected by a neurodegenerative disease, researchers can identify specific metabolites and pathways involved in disease progression and pathogenesis4.One of the critical applications of metabolomics is the identification of biomarkers for early diagnosis. Metabolic changes often precede clinical symptoms, making metabolomic biomarkers valuable for early detection. Mendelian randomization can identify metabolic, proteomic, or other biological markers that are causally related to neurodegenerative diseases. For instance, genetic variants influencing levels of specific metabolites or proteins can be tested for their association with disease risk, helping to pinpoint biomarkers involved in disease etiology3.

By establishing a causal link between a biomarker and disease, mendelian randomization supports the development of early detection tools6. Biomarkers identified through MR can be used to screen for neurodegenerative diseases before clinical symptoms appear, enabling earlier intervention and management7.

Method: Sample preparation

We collected 50 serum samples of healthy control people and 50 serum samples of patients with Parkinson's disease. 100 µL sample was thoroughly mixed with 400 µL of cold methanol acetonitrile (v/v, 1:1) via vortexing. And then the mixture were processed with sonication for 1 h in ice baths. The mixture

was then incubated at -20°C for 1 h, and centrifuged at 4 °C for 20 minutes with a speed of 14, 000 g. The supernatants were then harvested and dried under vacuum LC-MS analysis.

UHPLC-MS/MS analysis

Metabolomics profiling was analyzed using a UPLC-ESI-Q-Orbitrap-MS system (UHPLC, Shimadzu Nexera X2 LC-30AD， Shimadzu，Japan) coupled with Q-Exactive Plus (Thermo Scientific, San Jose, USA).

The flow rate was 0.5 mL/min and the mobile phase contained: A: 25 mM ammonium acetate and 25 mM ammonium hydroxide in water and B: 100% acetonitrile (ACN). The gradient was 95% B for 1 min and was linearly reduced to 65% in 7 min, and then reduced to 35% in 2 min and maintained for 1 min, and then increased to 95% in 0.5 min, with 2 min re-equilibration period employed. Both electrospray ionization (ESI) positive-mode and negative mode were applied for MS data acquisition. The HESI source conditions were set as follows: Spray Voltage：3.8kv（+）和3.2kv（-）；Capillary Temperature：320（±）；Sheath Gas：30（±）；Aux Gas：5（±）；Probe Heater Temp：350（±）；S-Lens RF Level：50. In MS only acquisition, the instrument was set to acquire over the m/z range 80-1200 Da. The full MS scans were acquired at a resolution of 70,000 at m/z 200, and 17,500 at m/z 200 for MS/MS scan. The maximum injection time was set to for 100 ms for MS and 50 ms for MS/MS. The isolation window for MS2 was set to 2 m/z and the normalized collision energy (stepped) was set as 27, 29 and 32 for fragmentation.

Serum metabolite GWAS data sources

GWAS data pertaining to the human serum metabolite Behenoyl dihydrosphingomyelin (d18:0/22:0) levels was retrieved from the metabonomics GWAS server, which is available at http://www.ebi.ac.uk/gwas/. The specified accession number for the relevant European GWAS datasets is GCST90200059. This genetic association data originates from a meta-analysis performed by Chen et al. It has been confirmed that all GWAS data were acquired from various consortia or organizations, guaranteeing that there is no overlap among the samples used.

Statistical analysis

The statistical evaluations were executed with the aid of R software (version 4.2.0, accessible at http://www.r-project.org) alongside the "two-sample MR" package (version 0.5.6) which facilitated the Mendelian randomization (MR) analyses 8. The underlying assumptions of the MR approach were verified via various sensitivity analyses and statistical tests. Heterogeneity across the chosen instrumental variables (IVs) was ascertained using the Cochran's Q test and its associated p-values. Should the null hypothesis of no heterogeneity be discarded, a random effects inverse-variance weighting (IVW) technique would supplant the fixed-effects IVW model 9. To address the issue of possible horizontal pleiotropy, the MR-Egger regression was employed. If the intercept of the Egger regression is significantly deviating from zero, it suggests the presence of horizontal pleiotropy 10. Furthermore, the MR-PRESSO method from the distinct MR-PRESSO package was utilized to detect and exclude any influential outliers that might distort the analysis results 11. To confirm the stability and influence of individual SNPs on the cumulative causal inference, a leave-one-out analysis was conducted.

Results: In terms of data stability, there were no statistical differences between healthy control individuals and Parkinson's Disease (PD) patients regarding the distribution of sex, age, education,

smoking status, or family history of PD. Principal Component Analysis (PCA) indicated R2X = 0.434 and Q2 = 1.187 (Fig 1), while Partial Least Squares Discriminant Analysis (PLS-DA) showed Q2 = 0.94 (Fig 2). VIP score > 1.0 was used as the screening criterion, Orthogonal PLS-DA (OPLS-DA) demonstrated Q2 = 0.885. The results from PCA, PLS-DA, and OPLS-DA confirm that the data possesses predictive capability. Our metabolomics approach identified 324 serum metabolites in both controls and patients (Fig 3).

We first conducted Mendelian randomization analysis on serum metabolites in PD patients, which revealed a correlation between sphingomyelin metabolites and the onset of PD. Consistent with these results, LC-MS-based serum metabolomics indicated significant statistical differences in several phospholipid metabolites between healthy individuals and PD patients. Specifically, dihydrosphingosine (log2FC = -0.22, FC = 0.85, $p < 0.05$) and phytosphingosine (log2FC = 0.28, FC = 1.22, $p < 0.05$) were found to differ significantly, with phytosphingosine levels decreased and dihydrosphingosine levels increased in PD patients. These compounds show potential as biomarkers for PD detection. Additionally, PD patients exhibited lower levels of methyl gallate, reserpine, toddalolactone, acetoacetate, and 1-methyladenosine compared to healthy controls. Conversely, higher levels of isoferulic acid, vanillin acetate, histamine, P-coumaraldehyde, and 4-methylumbelliferone were observed in PD patients.

The identified 324 metabolites primarily belong to three categories: alkaloids, prenol lipids, terpenoids, and phospholipid metabolites (Fig 4). Specifically, 10 alkaloid metabolites showed differences between the groups, including hydroquinidine (log2FC = 0.96, FC = 1.95), remerine (log2FC = 0.96, FC = 1.95), piperine, and ergonovine (log2FC = 1.59, FC = 3.02). Among the prenol lipids, 5 metabolites differed, such as rhodopin (log2FC = 2.02, FC = 1.95), alpha-carotene (log2FC = 1.66, FC = 3.67), and mactraxanthin (log2FC = -8.63, FC = 0.00). Additionally, 4 terpenoid metabolites showed differences, including arjungenin (log2FC = -8.63, FC = 0.00), canthaxanthin (log2FC = -8.78, FC = 0.00), and ursolic acid (log2FC = 1.08, FC = 2.12).

The functions of these 324 metabolites are primarily related to ferroptosis, glutathione metabolism, and tryptophan metabolism (Fig 5). Two metabolites associated with ferroptosis were significantly downregulated in PD patients: L-glutamic acid (log2FC = -0.48, FC = 0.72) and arachidonic acid (log2FC = -0.56, FC = 0.68). Oxidized glutathione (log2FC = 3.26, FC = 9.59), also linked to ferroptosis, was significantly upregulated in PD patients. Metabolites associated with glutathione metabolism that were significantly downregulated in PD patients included pyroglutamic acid (log2FC = 2.05, FC = 4.15), L-glutamic acid (log2FC = -0.48, FC = 0.72), and ascorbic acid (log2FC = 3.29, FC = 9.81). Additionally, two metabolites related to tryptophan metabolism, indole-3-acetaldehyde (log2FC = 0.20, FC = 1.14) and L-kynurenine (log2FC = 0.26, FC = 1.19), were significantly downregulated in PD patients.

In this study, we applied the mendelian randomization and untargeted LC-MS metabolomic approach to investigate the changes in biochemical pathways related to PD . The mendelian randomization unveiled the relationship between sphingomyelin and PD. Untargeted LC-MS metabolomic approach further validated this result. In addition, metabolomic profiling of the serum samples from PD patients and healthy people revealed significantly altered levels of metabolites belonging to the class of alkaloids, prenol lipids, terpenoids, steroids, carbohydrates, phospholipid metabolites. Through bioinformatics analysis of these metabolites, it is indicated that compared with healthy patients, PD patients exhibit dysfunction in ferroptosis, glutathione metabolism, tryptophan metabolism, synaptic cycle, suggesting potential, easily accessible, diagnostic and prognostic metabolomic biomarkers of PD.

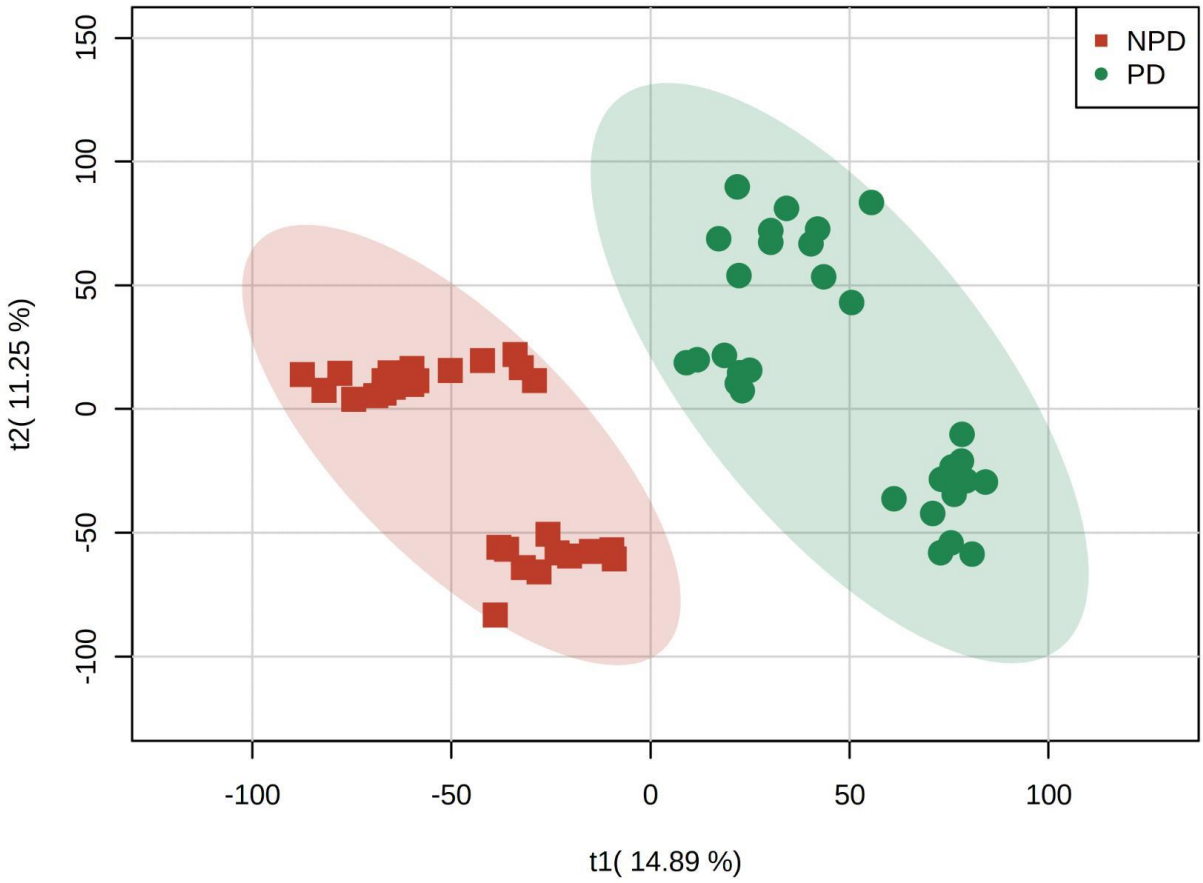
NPD
PD
150
100
50
0
-50
-100
t2(11.25 %)
-100
-50
0
50
100
t1(14.89 %)

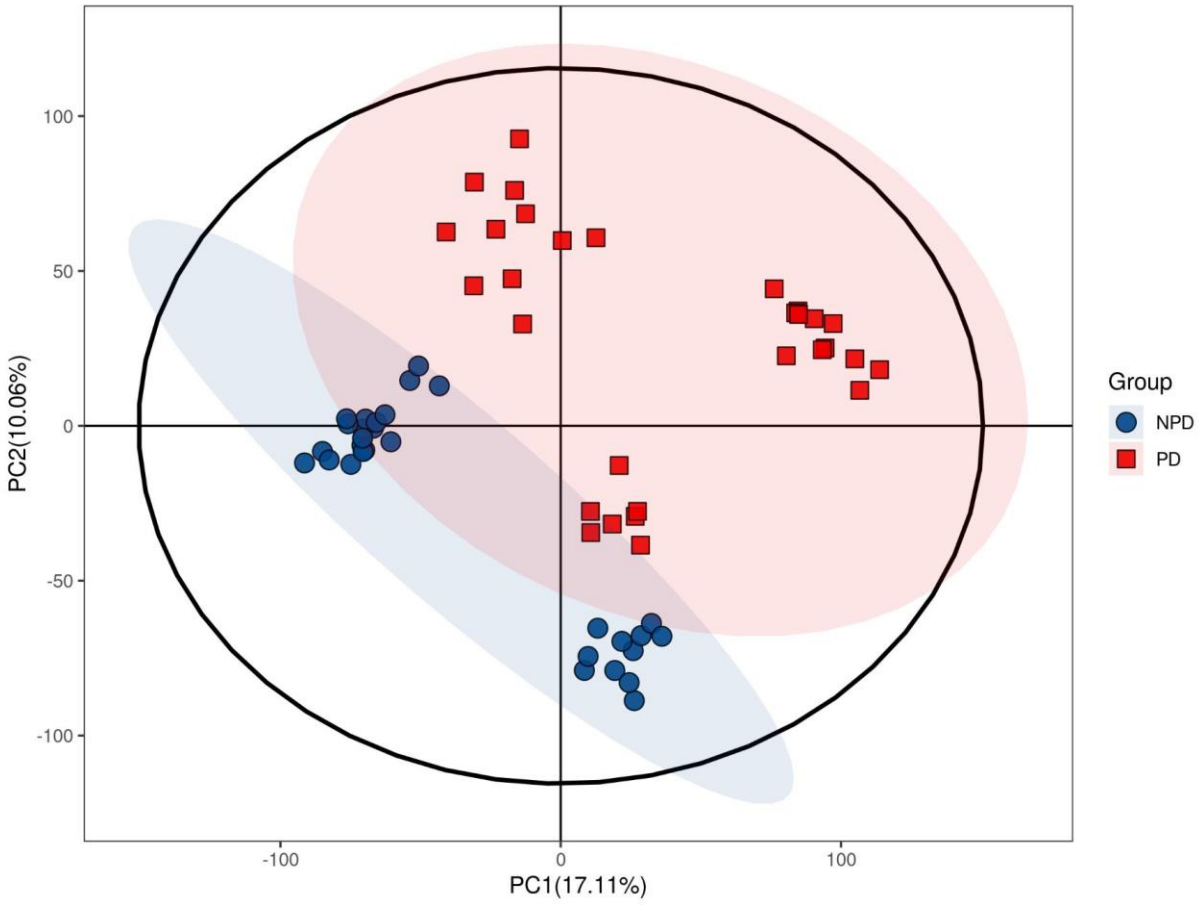
100
50
0
-50
-100
PC2(10.06%)
-100
0
100
PC1(17.11%)
Group
NPD
PD

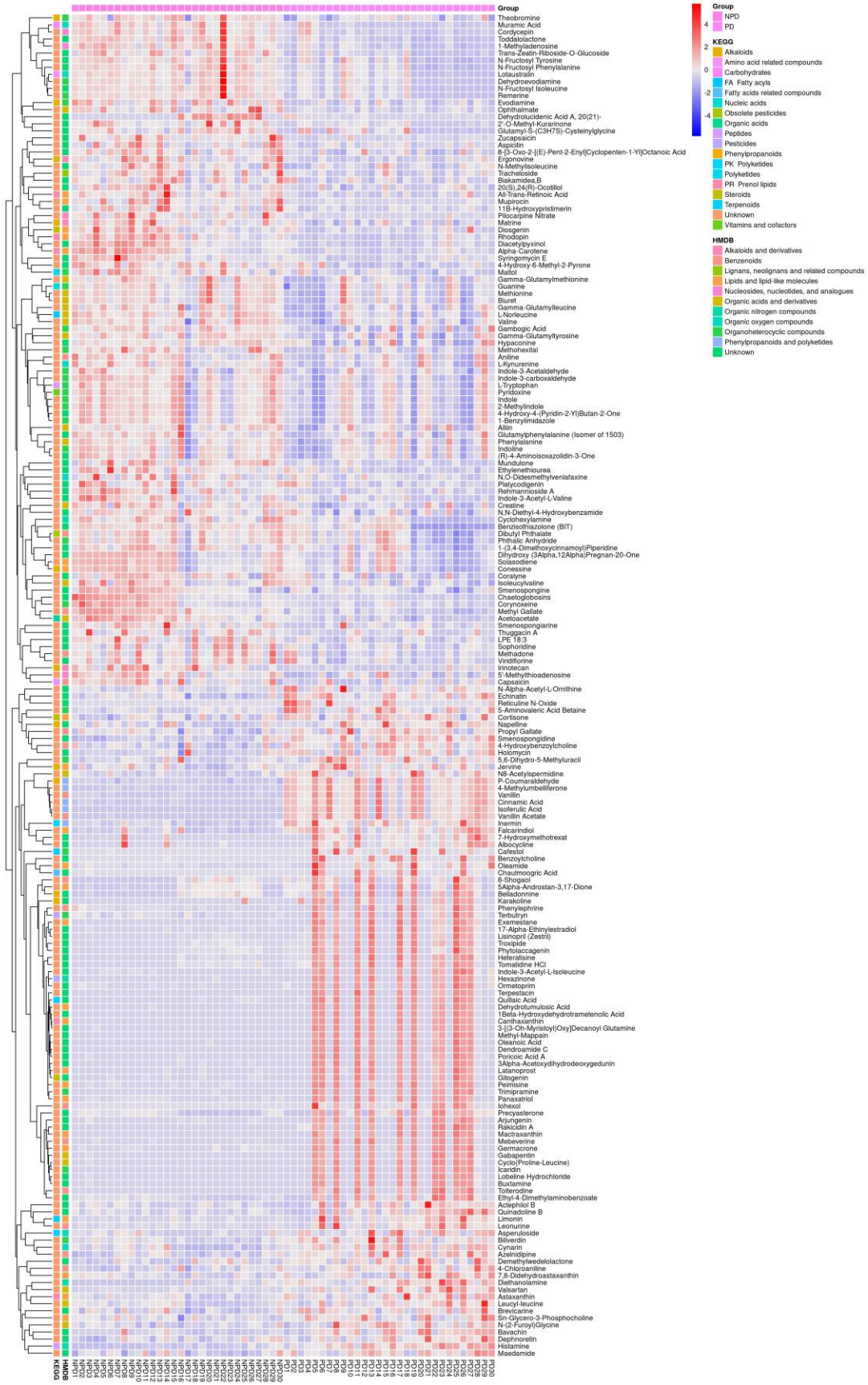
Group
Theobromine
Muramic Acid
Cordycepin
Toddalolactone
1-Methyladenosine
Trans-Zeatin-Riboside-O-Glucoside
N-Fructosyl Tyrosine
N-Fructosyl Phenylalanine
Lotaustralin
Dehydroanvodiamine
N-Fructosyl Isoleucine
Remerine
Evodiamine
Ophthalmate
Dehydrolucidenic Acid A, 20(21)-
2'-O-Methyl-Kurarinone
Glutamyl-S-(C3H7S)-Cysteinylglycine
Zucapsaicin
Aspicilin
8-[3-Oxo-2-[(E)-Pent-2-Enyl]Cyclopenten-1-Yl]Octanoic Acid
Ergonovine
N-Methylisoleucine
Tracheloside
Biakamidea,B
20(S),24(R)-Ocotillol
All-Trans-Retinoic Acid
Mupirocin
11Β-Hydroxypristimerin
Pilocarpine Nitrate
Matrine
Diosgenin
Rhodopin
Diacetylpyxinol
Alpha-Carotene
Syringomycin E
4-Hydroxy-6-Methyl-2-Pyrone
Maltol
Gamma-Glutamylmethionine
Guanine
Methionine
Biuret
Gamma-Glutamylleucine
L-Norleucine
Valine
Gambogic Acid
Gamma-Glutamyltyrosine
Hypaconine
Methohexital
Aniline
L-Kynurenine
Indole-3-Acetaldehyde
Indole-3-carboxaldehyde
L-Tryptophan
Pyridoxine
Indole
2-Methylindole
4-Hydroxy-4-(Pyridin-2-Yl)Butan-2-One
1-Benzylimidazole
Alliin
Glutamylphenylalanine (Isomer of 1503)
Phenylalanine
Indoline
(R)-4-Aminoisoxazolidin-3-One
Mundulone
Ethylenethiourea
N,O-Didesmethylvenlafaxine
Platycodigenin
Rehmannioside A
Indole-3-Acetyl-L-Valine
Creatine
N,N-Diethyl-4-Hydroxybenzamide
Cyclohexylamine
Benzisothiazolone (BIT)
Dibutyl Phthalate
Phthalic Anhydride
1-(3,4-Dimethoxycinnamoyl)Piperidine
Dihydroxy (3Alpha,12Alpha)Pregnan-20-One
Solasodiene
Conessine
Coralyne
Isoleucylvaline
Smenospongine
Chaetoglobosins
Corynoxeine
Methyl Gallate
Acetoacetate
Smenospongiarine
Thuggacin A
LPE 18:3
Sophoridine
Methadone
Viridiflorine
Irinotecan
5'-Methylthioadenosine
Capsaicin
N-Alpha-Acetyl-L-Ornithine
Echinatin
Reticuline N-Oxide
5-Aminovaleric Acid Betaine
Cortisone
Napelline
Propyl Gallate
Smenospongidine
4-Hydroxybenzoylcholine
Holomycin
5,6-Dihydro-5-Methyluracil
Jervine
N8-Acetylspermidine
P-Coumaraldehyde
4-Methylumbelliferone
Vanillin
Cinnamic Acid
Isoferulic Acid
Vanillin Acetate
Inermin
Falcarindiol
7-Hydroxymethotrexat
Albocycline
Cafestol
Benzoylcholine
Oleamide
Chaulmoogric Acid
8-Shogaol
5Alpha-Androstan-3,17-Dione
Belladonnine
Karakoline
Phenylephrine
Terbutryn
Exemestane
17-Alpha-Ethinylestradiol
Lisinopril (Zestril)
Troxipide
Phytolaccagenin
Heteratisine
Tomatidine HCl
Indole-3-Acetyl-L-Isoleucine
Hexazinone
Ormetoprim
Terpestacin
Quillaic Acid
Dehydrotumulosic Acid
1Beta-Hydroxydehydrotrametenolic Acid
Canthaxanthin
3-[(3-Oh-Myristoyl)Oxy]Decanoyl Glutamine
Methyl-Mappain
Oleanoic Acid
Dendroamide C
Poricoic Acid A
3Alpha-Acetoxydihydrodeoxygedunin
Latanoprost
Glitogenin
Peimisine
Trimipramine
Panaxatriol
Iohexol
Precyasterone
Arjungenin
Rakicidin A
Mactraxanthin
Mebeverine
Germacrone
Gabapentin
Cyclo(Proline-Leucine)
Icaridin
Lobeline Hydrochloride
Buxtamine
Tolterodine
Ethyl-4-Dimethylaminobenzoate
Actephilol B
Quinadoline B
Limonin
Leonurine
Asperuloside
Biliverdin
Cynarin
Azelnidipine
Demethylwedelolactone
4-Chloroaniline
7,8-Didehydroastaxanthin
Diethanolamine
Valsartan
Astaxanthin
Leucyl-leucine
Brevicarine
Sn-Glycero-3-Phosphocholine
N-(2-Furoyl)Glycine
Bavachin
Dephnoretin
Histamine
Maedamide
Group
NPD
PD
KEGG
Alkaloids
Amino acid related compounds
Carbohydrates
FA Fatty acyls
Fatty acids related compounds
Nucleic acids
Obsolete pesticides
Organic acids
Peptides
Pesticides
Phenylpropanoids
PK Polyketides
Polyketides
PR Prenol lipids
Steroids
Terpenoids
Unknown
Vitamins and cofactors
HMDB
Alkaloids and derivatives
Benzenoids
Lignans, neolignans and related compounds
Lipids and lipid-like molecules
Nucleosides, nucleotides, and analogues
Organic acids and derivatives
Organic nitrogen compounds
Organic oxygen compounds
Organoheterocyclic compounds
Phenylpropanoids and polyketides
Unknown

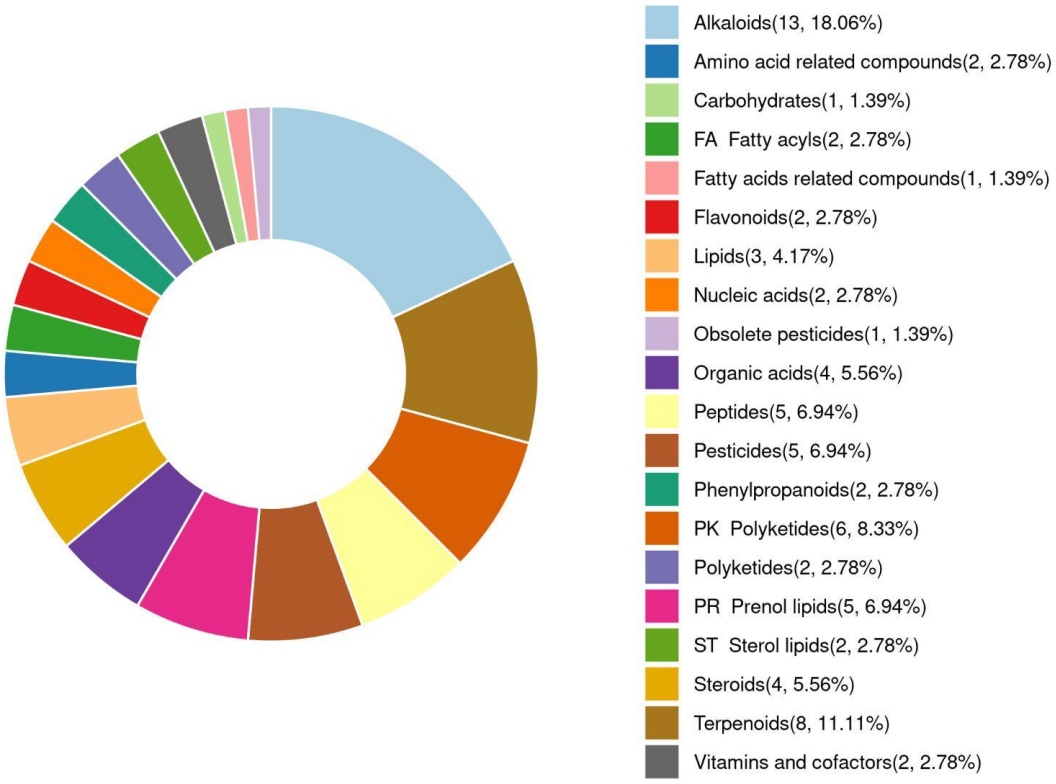
Alkaloids(13, 18.06%)
Amino acid related compounds(2, 2.78%)
Carbohydrates(1, 1.39%)
FA Fatty acyls(2, 2.78%)
Fatty acids related compounds(1, 1.39%)
Flavonoids(2, 2.78%)
Lipids(3, 4.17%)
Nucleic acids(2, 2.78%)
Obsolete pesticides(1, 1.39%)
Organic acids(4, 5.56%)
Peptides(5, 6.94%)
Pesticides(5, 6.94%)
Phenylpropanoids(2, 2.78%)
PK Polyketides(6, 8.33%)
Polyketides(2, 2.78%)
PR Prenol lipids(5, 6.94%)
ST Sterol lipids(2, 2.78%)
Steroids(4, 5.56%)
Terpenoids(8, 11.11%)
Vitamins and cofactors(2, 2.78%)

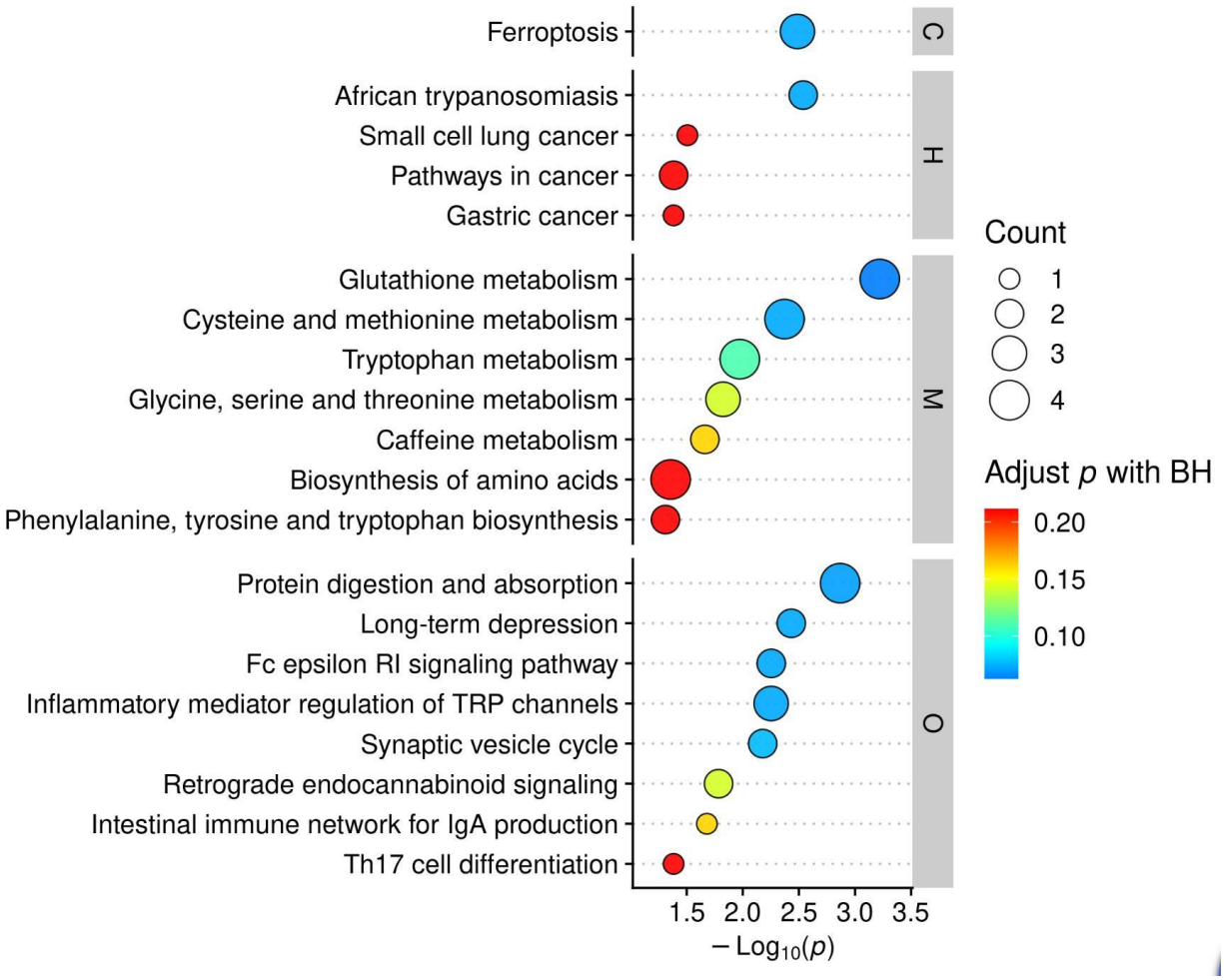

LBA-6: Frequency-selective suppression of essential tremor via transcutaneous spinal cord electrical stimulation

A. Pascual-Valdunciel; J. Ibanez; L. Rocchi; J. Song; J. Rothwell; K. P. Bhatia; D. Farina; A. Latorre (London, United Kingdom)

Objective: This study aimed to investigate the potential of transcutaneous spinal cord electrical stimulation to suppress essential tremor in a frequency-dependent manner

Background: Essential tremor is a common and debilitating condition, yet current treatments often fail to provide satisfactory relief. Transcutaneous spinal cord electrical stimulation has emerged as a potential non-invasive neuromodulation technique capable of disrupting the oscillatory activity underlying tremors.

Method: Eighteen essential tremor patients completed the study. The experiment consisted of 60 s postural tremor recording, during 5 conditions: no stimulation, transcutaneous spinal cord electrical stimulation at tremor frequency, transcutaneous spinal cord electrical stimulation at 1 Hz, transcutaneous spinal cord electrical stimulation at 21 Hz and trapezius stimulation (serving as a control). Tremor frequency and amplitude were analysed and compared across the conditions.

Results: We found tremor amplitude reduction at tremor frequency stimulation, during the entire trial but significant only during the second half of the stimulation. This result was reinforced by the observation that the same stimulation resulted in the highest number of responders. Transcutaneous spinal cord electrical stimulation at 1 Hz showed a trend toward decreased tremor amplitude in the latter half of stimulation, though this trend did not reach statistical significance. Stimulation at 21 Hz did not produce any significant alterations in tremor, while trapezius stimulation exacerbated it. Notably, during tremor frequency stimulation, a subgroup of responders exhibited consistent synchronization between tremor phase and delivered stimulation, indicating tremor entrainment.

Cervical transcutaneous spinal cord electrical stimulation holds promise for alleviating postural tremor in essential tremor patients when delivered at the subject's tremor frequency. The observed changes in tremor amplitude likely result from the modulation of spinal cord circuits by transcutaneous spinal cord electrical stimulation, which disrupts the oscillatory drive to muscles by affecting afferent pathways or spinal reflexes. However, the possibility of an interplay between spinal and supraspinal centres cannot be discounted

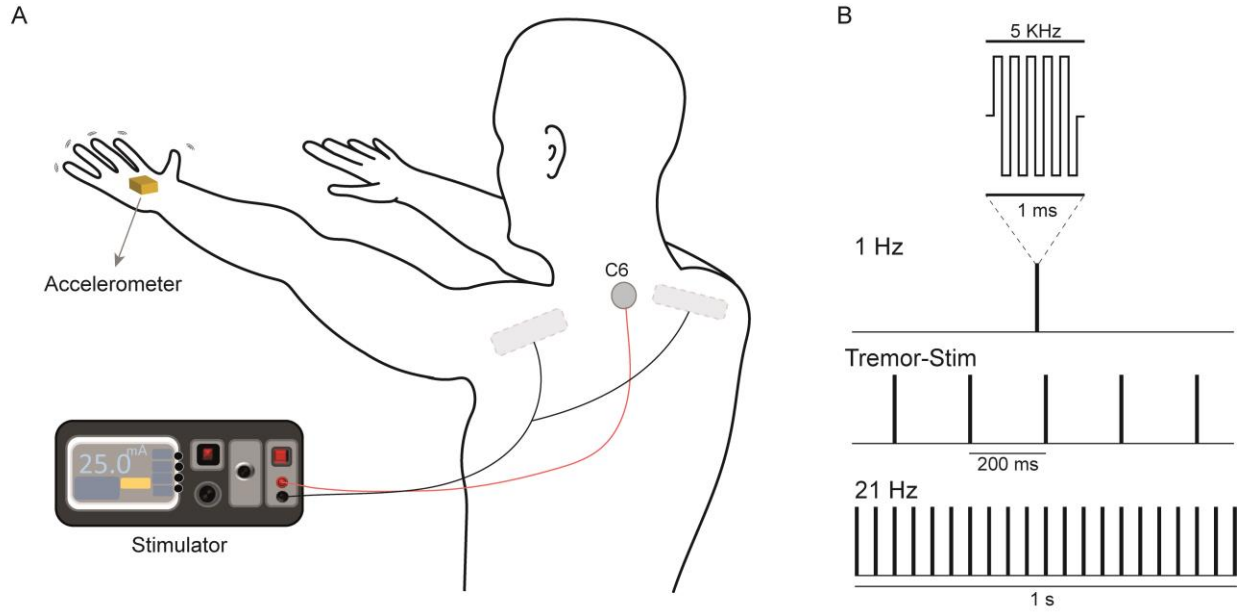

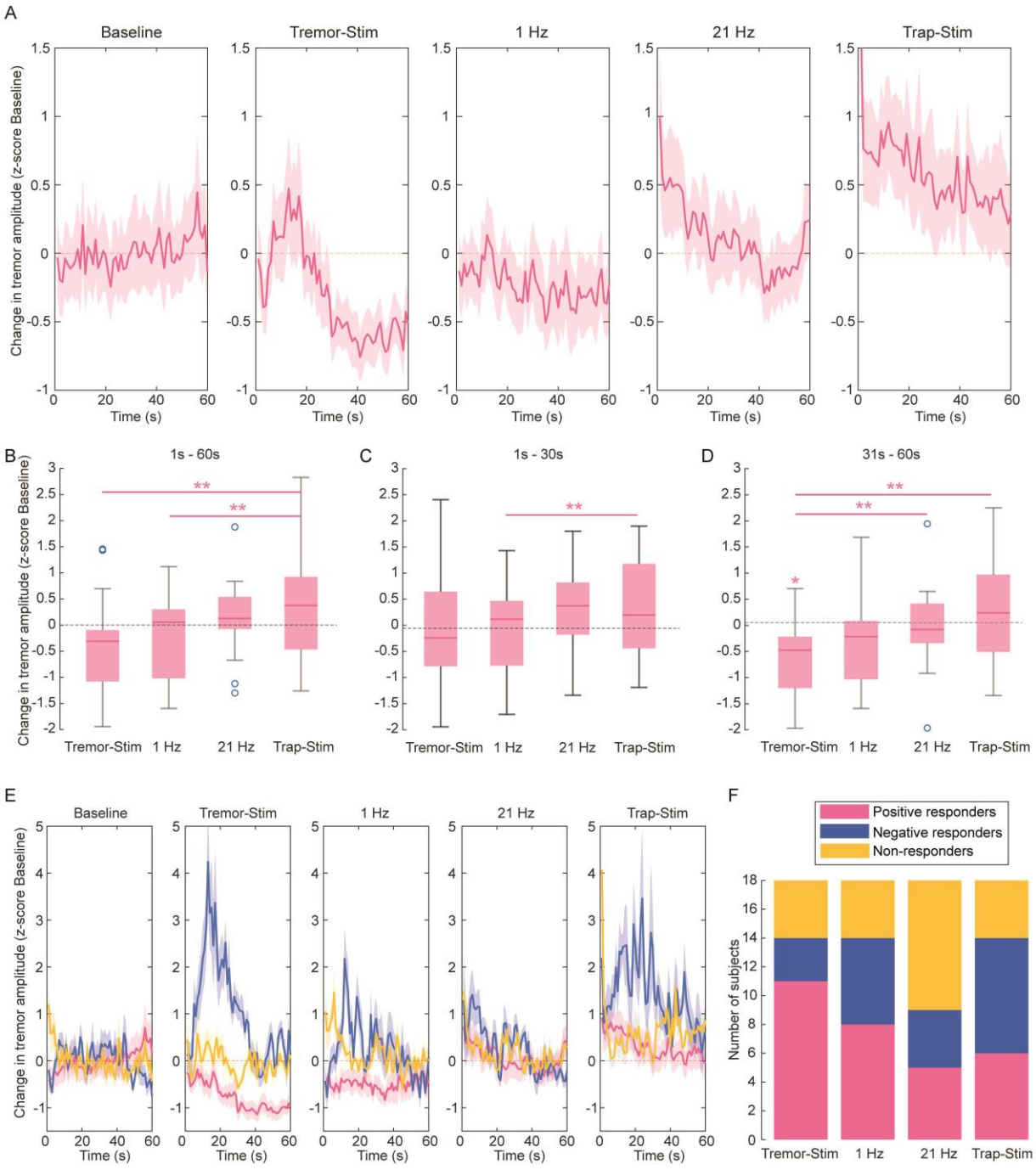
A
Baseline
Tremor-Stim
1 Hz
21 Hz
Trap-Stim
Change in tremor amplitude (z-score Baseline)
Time (s)
B
1s - 60s
C
1s - 30s
D
31s - 60s
**
*
Tremor-Stim
1 Hz
21 Hz
Trap-Stim
E
F
Positive responders
Negative responders
Non-responders
Number of subjects

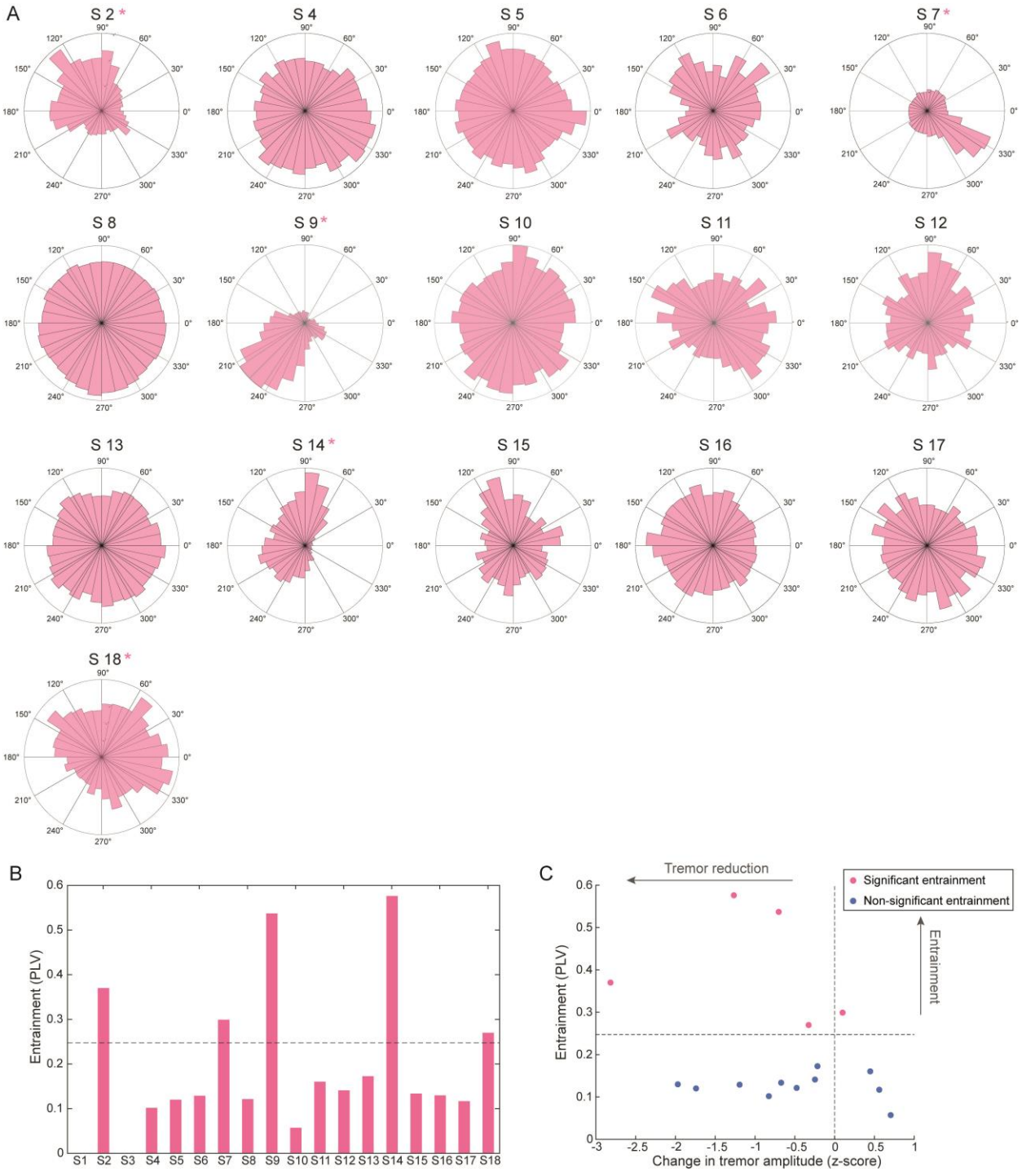

LBA-7: Diving into Health: Revolutionizing Parkinson's Disease Rehabilitation with Aquatic HIIT

F. Nazemi; A. Chitsaz; N. Salimian; A. Alipur Shehni; S. Ahmadi (Isfahan, Iran)

Objective: To investigate the effects of aquatic high-intensity interval training (HIIT) on balance, physical function and sarcopenia in patients with Parkinson's disease (PD).

Background: Parkinson's disease is a progressive neurodegenerative disorder characterized by debilitating motor symptoms such as tremors, rigidity, and bradykinesia, as well as non-motor symptoms that profoundly impact patients' quality of life. Traditional pharmacological treatments primarily manage symptoms but do not slow disease progression. Exercise, particularly high-intensity interval training, has garnered attention for its potential to enhance neuroplasticity, improve physical function, and boost overall health in PD patients. However, land-based HIIT can be challenging and risky for individuals with balance and mobility impairments. Some studies including participants with neurological and metabolic conditions tend to experience a higher rate of withdrawal and adverse events following the HIIT program (on land) than with a control exercise program, which could be a concern when implementing programs.

While land-based High-Intensity Interval Training (HIIT) presents challenges for those with balance and mobility impairments, it is particularly risky for individuals with Parkinson's disease due to their susceptibility to falls and injuries. The aquatic environment offers a safer alternative for HIIT, accommodating the specific needs of Parkinson's patients. The buoyant nature of water can alleviate joint stress and aid in performing movements that are challenging on land, making it an ideal medium for HIIT among people with chronic conditions. The water's resistance can also contribute to strengthening muscles. This adaptation is crucial for Parkinson's patients, who often struggle with rigidity and bradykinesia, as it allows them to perform exercises at higher intensities with reduced risk of injury. This reduced loading may also make exercise can lead to more effective, feasible, and enjoyable exercise experiences, especially for those who find land-based training difficult, thus encouraging better adherence. Additionally, the aquatic environment allows those with restricted mobility to engage in more intense training than they could on land. There are many barriers to exercise, including symptoms and function, and common problems among people with chronic conditions especially neuromuscular disorders are immobility, pain and fatigue. Furthermore, there is a potential for nonadherence due to joint and muscle injury with land-based HIIT. There may be a potential in reducing some of these barriers to exercise in the water to facilitate improved longer-term adherence to training programs. Aquatic HIIT, characterized by bursts of intense activity in a water setting, offers a unique combination of cardiovascular and resistance training, which may be particularly beneficial for PD patient.

Previous studies have demonstrated the benefits of aquatic exercise for various health conditions, yet its specific effects on Parkinson’s disease remain underexplored. This study addresses this gap by evaluating the benefits of a structured aquatic HIIT program for individuals with Parkinson’s disease.

Method: A randomized controlled trial was conducted with 56 Parkinson’s disease patients, aged 55-75 years, randomly assigned to either the aquatic HIIT group (n=28) or the control group (n=28). The aquatic HIIT group participated in a 8-week program consisting of trice weekly sessions. Each session included a warm-up, followed by high-intensity intervals of aquatic exercises (e.g., water running, aquatic jumping jacks, and resistance exercises with water weights), interspersed with low-intensity recovery periods. The control group received standard care without specific exercise intervention.

Baseline and post-intervention assessments were conducted to measure balance (using the Berg Balance Scale), physical function (using short physical performance battery (SPPB)), and sarcopenia (measuring muscle mass by using bioelectrical impedance analysis and measuring muscle strength by grip strength). Statistical analysis compared pre- and post-intervention changes between the two groups.

Results: The aquatic HIIT group demonstrated significant improvements in all measured parameters compared to the control group. Balance scores increased by an average of 25% ($p < 0.05$), reflecting enhanced stability and a reduced risk of falls. Physical function scores also show 30% improvement ($p < 0.01$), highlighting the effectiveness of aquatic training. Additionally, there was a notable significant increase in average skeletal muscle mass ($p < 0.05$), and a 21% increase in muscle strength ($p < 0.05$). The control group showed no significant changes in any of the measured outcomes.

Aquatic high-intensity interval training is a transformative and safe exercise modality for patients with Parkinson's disease, offering substantial improvements in balance, physical function, and sarcopenia indices. The unique properties of water create an ideal environment for intense physical activity, significantly reducing the risk of injury and promoting patient adherence. This study highlights the potential of aquatic HIIT to revolutionize physical rehabilitation for PD patients, providing a powerful adjunct to traditional therapeutic strategies. Implementing such programs could markedly enhance the quality of life and functional independence for individuals living with Parkinson's disease, representing a significant advancement in the management of this challenging condition. Future research should focus on long-term adherence to aquatic HIIT and its effects on disease progression in Parkinson's patients.

LBA-8: 3 Classification of alpha synuclein aggregation in the brain by neural derived EV-bound biomarkers in blood in Parkinson's Disease

G. Ho; R. Samat; P. Maimonis; M. Marken; M. Cantillon

Objective: To evaluate brain alpha synuclein in simple blood test

Background: In the absence of gold standard neuroimaging as amyloid PET in AD, diagnostic and progression markers in Parkinson's disease are needed. Neither in CSF , nor in blood total α-synuclein has proven to a reliable diagnostic , with significant variations in its concentration (Shi et al., 2014), while CSF RTQuick seeding amplification and skin biopsies allow only a binary result. Emerging research suggests that Glial and Neuronal extracellular vesicles play a crucial role in transferring alpha-synuclein aggregates throughout the brain [Danzer, 2012; Guo, 2020]. EVs carrying proteins can freely traverse the blood-brain barrier, either through transcytosis or targeted uptake by endothelial cells. Our earlier clinical studies indicate that direct measurement of biomarkers associated with neural derived EVs in the bloodstream, as here , do provide a more accurate measure of brain-related abnormalities compared to soluble proteins.

Method: Blood samples were collected from Parkinson's Disease diagnosed patients (n=16) and age matched healthy controls (n=24) with informed consent. Blood samples were collected by venipuncture into EDTA tubes using sterile techniques. Blood samples were centrifuged at 1500 x g for 10 minutes to separate plasma from cellular components. Plasma was then aspirated into sterile tubes and stored at -80°C until further analysis. In-house developed assays were performed to measure the amounts of neural EV-bound forms of alpha synuclein, GFAP, and NfL and soluble forms of the same proteins in the plasma samples.

Results: On this initial sample, the neural derived EV-bound NDEV alpha synuclein and GFAP in the plasma was able to distinguish between healthy and PD patients (AUC: 0.86). Soluble (non-EV bound) forms of the same biomarkers in blood were unable to do so (AUC: 0.56).Further cohorts are in analysis.

Neural derived EVs, that are measured directly in blood, contain forms of biomarkers as aggregated amyloid, tau or alpha synuclein relevant to their state in the brain in diseases such as AD and PD and allow easy access to screening.

LBA-9: First in Human Administration of an Autologous Investigational Cell Therapy for Parkinson Disease Using an Intraoperative MRI-guided Posterior Approach

C. Christine; N. Phielipp; M. Houser; S. Sherman; E. Wirth III (San Diego, CA, USA)

Objective: A first-in-human clinical trial was recently launched to evaluate the safety and tolerability of two sequential escalating doses of autologous induced pluripotent stem cell (iPSC)-derived dopaminergic neuron precursor cells (DANPC) in subjects with moderate to advanced Parkinson Disease.

Background: One key objective of this study is to evaluate the feasibility and safety of an intraoperative MRI (iMRI)-guided posterior approach, which potentially enables maximum distribution of the DANPC in the post-commissural putamen target site with the fewest possible cannula insertions. This has not been attempted in humans, but the feasibility and safety of this approach was recently demonstrated in a preclinical study in non-human primates (Emborg et al., J. Neurosurgery, in press).

Method: Administration of the DANPC was performed with the subject under general anesthesia in the prone position using a commercially available iMRI system. The DANPC were injected bilaterally in a single surgical procedure using a custom syringe and cannula that enabled delivery at a rate of 2-3 µL/minute. Intraoperative visualization of the cell deposits was aided by the addition of 1mM gadoteridol during preparation of the cells for injection. The first dose cohort (N=3) in this study received the initial planned dose of five million (5M) DANPC per putamen in a volume of 50 µL. This total volume was divided into two tracks of 25 µL/track, with the first track centered in the dorsal third of the putamen and the second track centered approximately 5mm ventral. Cell deposits were initiated at the level of the anterior commissure in the coronal plane and then spaced 2mm apart in the post-commissural putamen with the final deposit situated 2-3mm inside the posterior putaminal margin.

Results: The first three participants have completed 1-3 months of post-surgical follow-up. No intraoperative hemorrhages or serious surgical complications have been observed. The most common adverse event to date was mild to moderate tongue swelling in all 3 participants due to the surgical procedure in the prone position.

The results to date indicate that the initial dose of 5M DANPC can be safely administered to the post-commissural putamen using an iMRI-guided posterior approach and support dose escalation in the second cohort of participants.

LBA-10: The novel glucocerebrosidase chaperone GT-02287 in development for GBA-PD is safe and well tolerated in healthy volunteers at oral doses that produce plasma exposures in the projected therapeutic range

M. De Sciscio; M. Bosetti; P. Martin; S. Cano; B. Guzman; A. Marcinowicz; A. Rozwadowsk; A. Schreiner; N.Dzamko; J. Taylor; T. Ignoni; J. Hannestad (Bethesda, MD, USA)

Objective: To characterize the safety, tolerability, pharmacokinetics (PK), and pharmacodynamics of the small-molecule glucocerebrosidase (GCase) chaperone GT-02287 in healthy volunteers.

Background: Pathogenic variants in the GBA1 gene, which encodes for the lysosomal enzyme GCase, constitute the most common genetic risk factor for Parkinson's disease and are associated with more rapid motor progression and increased risk of developing dementia. GBA1 variants impact the endolysosomal trafficking of GCase, which leads to endoplasmic reticulum (ER) stress, lysosomal dysfunction, impaired autophagy, reduced GCase enzymatic activity, mitochondrial dysfunction, neuroinflammation, and alpha-synuclein aggregation. GT-02287 is an orally-bioavailable investigational small molecule that was designed to bind to an allosteric site on GCase and act as a chaperone, facilitating the transport of GCase from the ER to lysosomes and mitochondria, enhancing GCase activity.

Method: Healthy male (n=40) and female (n=33) volunteers were enrolled in this Phase 1 first-in-human study and randomized within each cohort in a 3:1 ratio to active GT-02287 or placebo. Single oral doses of 2.4, 4.8, 7.7, 10, and 15 mg/kg and multiple oral doses of 4.8, 7.7, 10, and 13.5 mg/kg (once a day for 14 days) were tested. Clinical laboratory tests, vital signs, ECG recordings, and adverse events (AEs) were monitored to evaluate safety and tolerability, and plasma PK parameters were characterized. Pharmacodynamic biomarkers included changes in GCase activity in dry blood spots and peripheral blood mononuclear cells, and changes in levels of lysosomal markers as measured by Western blot in blood cells.

Results: All single and multiple dose levels tested were well tolerated. AEs were mild (90%) or moderate (10%) in intensity and limited in duration. The most common AEs were headache and nausea. No serious adverse events occurred, and no safety signals in laboratory tests, ECGs, or vital signs were observed. The PK profile of GT-02287 was linear across the tested dose ranges, and plasma exposures within the projected therapeutic range were achieved.

In this Phase 1 study in healthy volunteers, the novel GCase chaperone GT-02287 was well tolerated after single and multiple doses without any safety signals at oral doses that produced plasma exposures in the projected therapeutic range. These results support continued development of GT-02287 in a study aimed at determining whether this investigational medicine can modulate the relevant biology in patients with Parkinson's disease carrying a pathogenic GBA1 variant.

LBA-11: A Phase 3, Randomized, Assessor-blind, Active-Controlled Study of Pimavanserin in Comparison with Quetiapine in Parkinson's Disease Psychosis

B. Kathiriya; Y. Patidar; V. Patel,; A. Singhal; B. Patel; S. Choudhury; R. Varadarajulu; A. Pattojoshi; B. Solanki; A. Sharma; A. Pande; K. Parmar; S. Jayalekshmi; R. Mridula; N. Sundarachary; P. Walzade; S. Ramteke; D. Kumar; P. Kumar; D. Sonawane; P. Devkare; M. Rajurkar; D. Patil; P. Ghadge; S. Mehta (Mumbai, India)

Objective: To evaluate the antipsychotic efficacy and safety of Pimavanserin in comparison to Quetiapine in patients with Parkinson's Disease Psychosis (PDP).

Background: Psychosis affects up to 60% of PD patients. Atypical antipsychotics like Quetiapine is commonly used for the treatment of PDP with mixed benefits. Pimavanserin is a newer, non-dopaminergic, selective 5-HT2A inverse agonist/ antagonist which attenuates PDP symptoms with little risk of worsening motor function.

Method: This was a Phase 3, multi-centre, randomized, assessor-blind, parallel-group, active-controlled comparative study. Patients with idiopathic PD of duration ≥1 year, and Hoehn & Yahr stage ≤3, presence of visual and/or auditory hallucinations (H), and/or delusions (D) and on a stable dose(s) of anti-Parkinson's medication(s) for a least 4 weeks were randomized to either Pimavanserin (PMV, 34 mg OD) or Quetiapine (QTP, 25-200 mg/d) arm for 56 days. Efficacy was assessed on change from baseline (CFB) in Scale for the Assessment of Positive Symptoms (SAPS) – Parkinson's Disease (SAPS-PD) score, SAPS score, Unified Parkinson's Disease Rating Scale (UPDRS) Part II and Part III, Clinical Global Impression on Improvement & Severity (CGI-I & CGI-S), and Scales for Outcomes in Parkinson's disease – Sleep (SCOPA-Sleep) at Days 14,28,42&56. Safety was assessed on incidence of Treatment Emergent Adverse Events (TEAEs).

Results: 247 Indian patients with PDP (120 in PMV and 127 QTP arm) were enrolled. The mean duration of psychosis was 1.2 years. CFB in SAPS-PD 9-item score at Day 56 was -9.64 ± 5.66 in PMV arm and -8.37 ± 6.09 in QTP arm ($p<0.0001$ for both). Difference in SAPS-PD 9-item score between two arms was -1.27 (-2.77, 0.24) meeting the pre-defined non-inferiority margin of -0.9. Statistically significant CFB was observed in SAPS-PD 9-item score in both arms at all visits ($p<0.0001$). For other endpoints (SAPS-H+D, UPDRS II + III, CGI-I & S, SCOPA-Sleep), significant CFB at Day 56 was observed in both arms. A total of 27 TEAEs (9 in PMV and 18 in QTP arm) were reported in 26 (10.5%) patients. Most common TEAEs were nasopharyngitis (2.5%) in PMV arm and headache (3.9%) in QTP arm. 26 events were of mild intensity. One event 'Ischemic stroke' led to death in QTP arm which was unrelated to QTP.

Pimavanserin is non-inferior to Quetiapine in treating PDP without worsening of motor symptoms. Both the study drugs were well tolerated.

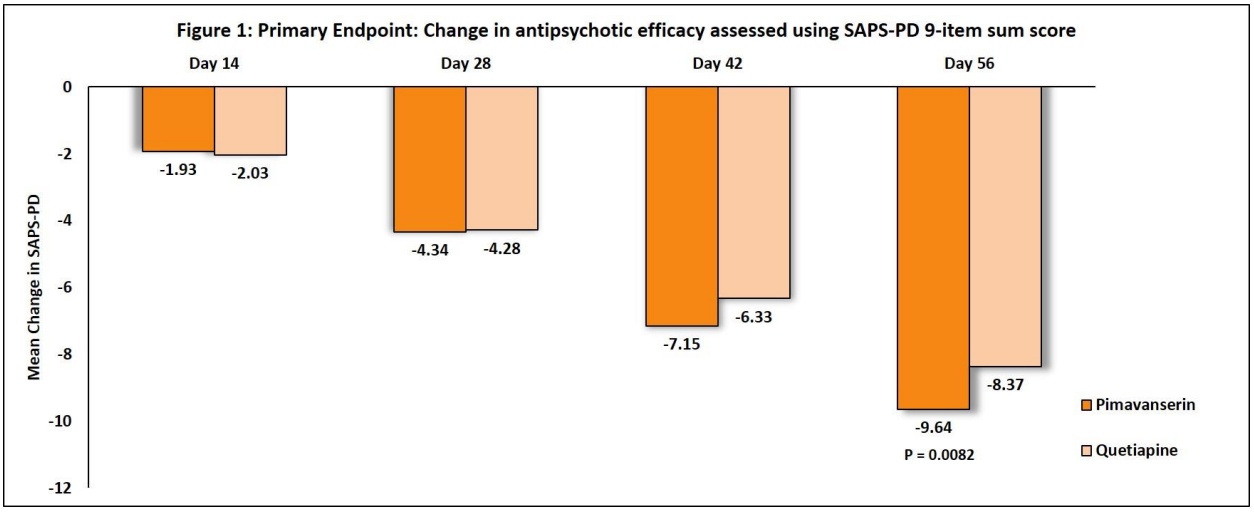

LBA-12: Efficacy and Safety of Tavapadon, an Orally Administered, Once-Daily, Selective D1/D5 Partial Dopamine Agonist, Adjunctive to Levodopa for Treatment of Parkinson's Disease With Motor Fluctuations

S. Isaacson; R. Last Name; P. Agarwal; W. Ondo; A. Park; L. Elmer; D. Kremens; M. Leoni; S. Duvvuri; C. Combs; E. Koenig; I. Chang; G. Pastino; S. Tringali; N. Golonski; R. Sanchez (Cary, NC, USA)

Objective: To evaluate the efficacy, safety, and tolerability of tavapadon as adjunctive therapy for motor fluctuations in levodopa-treated adults with Parkinson's disease (PD).

Background: Tavapadon is an investigational, once-daily, oral, selective D1/D5 partial dopamine agonist. Selective, partial agonism of D1/D5 receptors may provide the right balance of dopamine signaling to improve motor symptoms in PD while potentially minimizing certain adverse events (AEs) because tavapadon does not cause D2/D3 receptor activation or full D1/D5 agonism.

Method: TEMPO-3 (NCT04542499) is a phase 3, placebo-controlled, double-blind clinical trial evaluating tavapadon adjunctive to levodopa in adults with PD. Participants experiencing motor fluctuations (modified Hoehn and Yahr stage 2-3 in the ON state, minimum 2.5 h of OFF time on 2 consecutive diary days) receiving stable treatment with levodopa were randomly assigned (1:1) to receive adjunctive treatment with tavapadon (titrated to maximum tolerated flexible dose: 5–15 mg once daily) or placebo for 27 weeks. The primary endpoint was change from baseline in total daily ON time without troublesome dyskinesia (Hauser diary 2-day average; Week 26). Change from baseline in total daily OFF time and AEs were key secondary endpoints.

Results: Overall, 507 adults aged 40-80 years were enrolled. Participants receiving tavapadon (5–15 mg once daily) demonstrated a significant increase of 1.1 hours in total daily ON time without troublesome dyskinesia vs participants receiving placebo (1.7 hours vs 0.6 hours, respectively; $P<0.0001$). Change from baseline in daily OFF time also showed a significant reduction versus placebo. Tavapadon had an acceptable safety profile overall, consistent with prior clinical trials; the majority of AEs were mild to moderate in severity.

Findings from TEMPO-3 demonstrate the efficacy, tolerability, and acceptable safety profile of tavapadon when used adjunctive to levodopa for treatment of PD in adults with motor fluctuations. Ongoing phase 3 trials are evaluating the long-term use of tavapadon (open-label extension; TEMPO-4) and tavapadon as monotherapy in early PD (TEMPO-1 and TEMPO-2).

LBA-13: AI-based 3D anthropometric modeling for automated assessment and grading of dystonia patients

K. Dev Nayar; N. Ganza; S. Begalan; C. Go; A. Hunt; P. Acuna; N. Sharma (Boston, MA, USA)

Objective: Train a custom algorithm to adapt and fit 3D models to Dystonia patient videos and grade the cervical dystonia seen using the TWSTRS-2 questionnaire while following the scoring rubric.

Deriving the scores for the TWSTRS-2 scale in an XDP cohort and minimizing the deviation between the neurologist rating and the algorithm outputs.

Streamline a pathway to train a clinically-aligned foundation model that can understand the 3D anthropometric profile of the patient and have the ability to interpret and answer medical queries.

Background: Dystonia is the third most common movement disorder. It causes muscle contractions leading to repetitive movements and unusual postures, with cervical dystonia being the most prevalent form. Accurate assessment of its severity is crucial for treatment and drug development, typically relying on subjective scales like TWSTRS-2 and CDIP-58.

However, these require extensive physician training and are time-consuming to administer. Consequently, there's a growing need for objective and efficient evaluation methods. various technologies have been explored for objective measurement of cervical dystonia, from protractor collars to ultrasonography and specialized cameras. Despite their precision, these methods are time-intensive and may inadvertently affect dystonia symptoms as physical contact can alter the dystonia.

X-linked dystonia-parkinsonism (XDP) is a disease that manifests with symptoms of both Parkinson's disease and dystonia with varying progression. Due to the varying nature of the disease, it is important to be able to objectively document the course of the disease as it progresses and regresses through the symptoms of dystonia and parkinsonism.

There is a need for accurate evaluation tools. easy to set up, efficient, and contactless.

Method: We propose an AI-based approach based on ResNet-50 architecture, which models entities in patient videos into personalized 3-D meshes. This allows over 10,000 points on the patient's body to be tracked and therefore analyzed for movement disorders. For model evaluation, we have chosen the TWSTRS-2 questionnaire, and we intend to grade its severity subsection. The TWSTRS-2 questionnaire severity subscale has 6 different items, out of which we have graded - Maximal Excursion, Duration Factor, Range of motion, Shoulder elevation, and Time. Our patient cohort consists of 43 participants with X-linked dystonia Parkinsonism (XDP) who have been enrolled in a natural history study supported by the Collaborative Center for XDP (CCXDP) at Massachusetts General Hospital, the Sunshine Care Foundation, and Jose Reyes Memorial Medical Center. These participants have longitudinal video evaluations which have been graded for cervical dystonia severity utilizing the TWSTRS-2 questionnaire by expert neurologists. Participant videos were selected for stability, clarity, and completeness. The algorithm then graded the severity subsection of TWSTRS-2 after analyzing the videos.

Results: The predominant head posture involved more than one axis in 76% of participants and involved all three axes in 36.55%. Our metrics for head posture severity correlated with severity ratings from movement disorders neurologists using the TWSTRS-2 Rating Scale (rho = 0.85-0.91, $p < 0.001$).

Our algorithm’s convergent validity with clinical rating scales and reliance upon only conventional video recordings supports its further development and future potential for large-scale multi-site clinical trials. We further plan to encapsulate the AI algorithm as an evaluation tool for physicians to use in the clinics and for research.

LBA-14: The ki: SB-M Intelligibility Score — An Automatic Measure for Intelligibility in Motor Speech Disorders

F. Dörr; L. Schwed; N. Linz; A. König; T. Thies; M. Barbe; J. Orozco-Arroyave; J. Rusz (Saarbrucken, Germany)

Objective: To validate the ki: SB-M intelligibility score, a digital measure for speech intelligibility, across various motor speech disorders and languages in accordance with the Digital Medicine Society (DiMe) V3 framework.

Background: Dysarthria, a motor speech disorder resulting from muscle weakness or paralysis, significantly impairs speech intelligibility and quality of life. It is prevalent in conditions such as Parkinson's Disease (PD), atypical parkinsonism (e.g., progressive supranuclear palsy [PSP]), Huntington's Disease (HD), and amyotrophic lateral sclerosis (ALS). Enhancing and measuring intelligibility of speech is crucial for patients and serves as an important endpoint in clinical research and drug development.

Method: The study analyzed four datasets comprising healthy controls (HC) and patients with PD, HD, PSP, and ALS from Czech, Colombian, and German populations. Speech intelligibility was measured using the ki: SB-M intelligibility score, derived from automatic speech recognition (ASR) systems. Verification involved assessing inter-ASR reliability and temporal consistency. Analytical validation was conducted through correlations with gold standard clinical dysarthria scores for each disease. Clinical validation included group comparisons between HC and patients.

Results: Verification indicated good to excellent inter-rater reliability between ASR systems and fair to good temporal consistency. Analytical validation showed significant correlations between the SB-M intelligibility score and established clinical measures of speech impairment across all patient groups and languages. Clinical validation revealed significant differences in intelligibility scores between pathological groups and healthy controls, demonstrating the measure's discriminative capability.

The ki: SB-M intelligibility score is a reliable, valid, and clinically relevant tool for assessing speech intelligibility in motor speech disorders. It offers potential for enhancing clinical trials through automated, objective, and scalable assessments. Future research should investigate its utility in monitoring disease progression and therapeutic efficacy, as well as expand validation to include additional dysarthria cases.

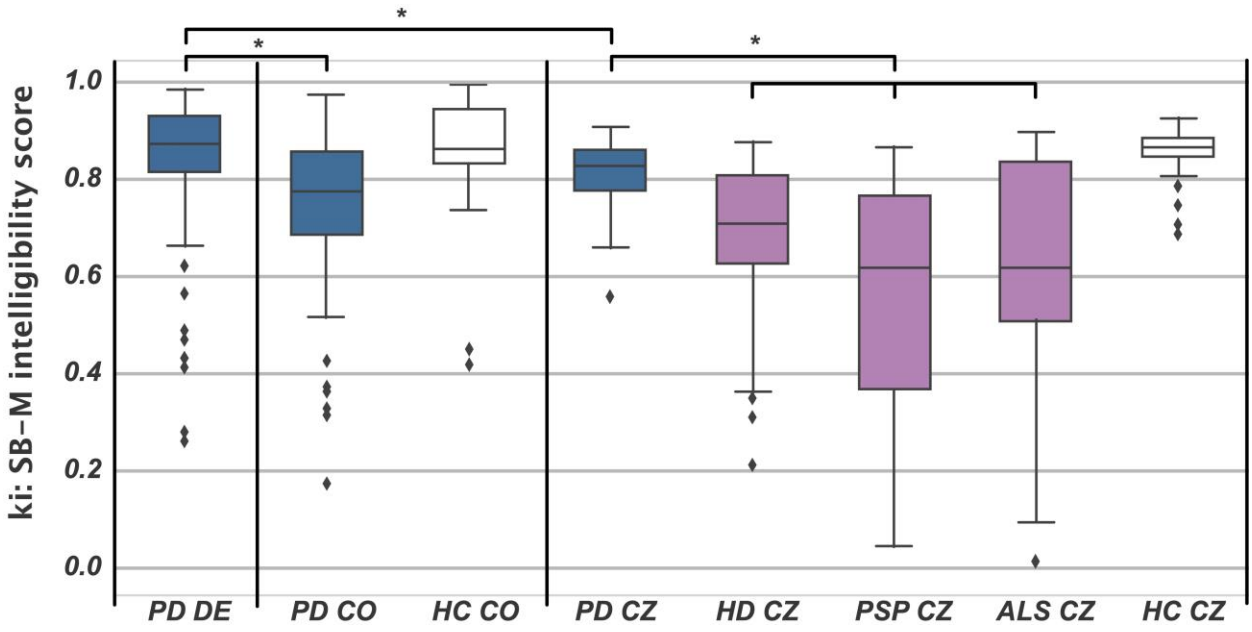

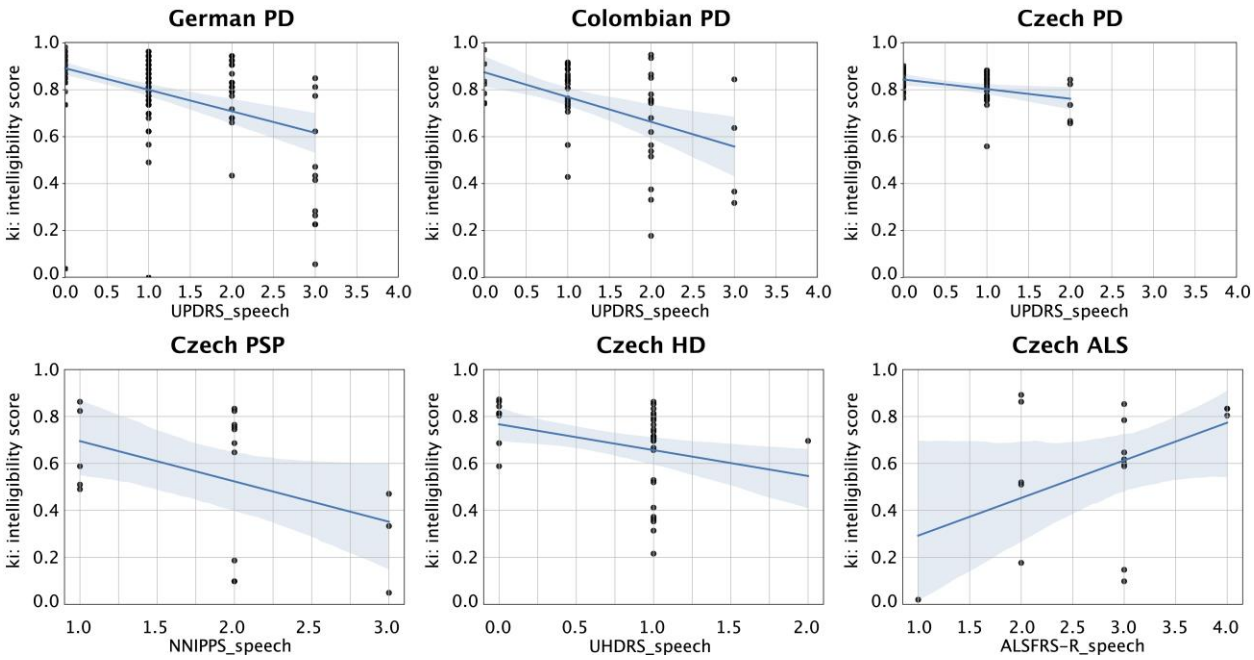

LBA-15: A Neuroimaging-Based Diagnostic Model of Parkinson's Disease Using Bootstrap Aggregating Deep Neural Network Classifiers

K. Van Hedger; N. Rothery; K. Seergobin; M. Elganga; D. Michels; A. Omar; H. Ganjavi; M. Khalil; A. Sarkar; P. MacDonald (London, ON, Canada)

Objective: We aimed to develop a diagnostic test of early Parkinson's disease (PD), using 3T MRI (T1w), diffusion MRI (dMRI), and a novel segmentation pipeline. We also tested if the model could distinguish patients with rapid eye movement sleep behaviour disorder (RBD). Our objective was to produce an automated diagnostic test with high clinical accuracy at the earliest disease stages.

Background: Accurate, accessible, and independently reproducible tests of PD are needed. Currently, diagnosis requires sub-specialists who are in short supply. These tests will improve the power of trials of disease-modifying therapies (DMTs).

Method: Data for this study (N=482, 217 female) were compiled from six datasets, most being multisite studies. Scans from PD [< 12 month since diagnosis; n=196; mean age=61.9(7.9)], RBD [n=84; mean age=66.4(5.0)], and healthy, age-matched controls [HC; n=202; mean age=64.4(6.2)], aged 45-75, were processed through our automated pipeline (Figure 1A). We extracted features from subcortical and cortical subregions. We pseudo-randomly selected 80% of our data for model development and 20% for an independent test (n=97). Using 5-fold cross-validation, we developed a diagnostic model using bootstrap aggregating deep neural network classifiers that embodies the concept of model averaging (reducing overfitting), as used in Bayesian statistics.

Results: Our binary classifier, in an independent hold-out set, distinguished early PD/RBD from HCs with high accuracy (ROC/AUC = 88), sensitivity = 0.89, and specificity = 0.83 (Figure 1B, 1C). Using more stringent thresholds, which encompassed approximately 80% of the data, accuracy ROC/AUC = 89, sensitivity = 0.95, and specificity = 0.84 improved further (Figure 1D). Subregions of subcortical structures most affected in PD (e.g., the caudal motor subregions of the striatum and substantia nigra

pars compacta) exerted greatest effect on our classifications, increasing confidence in the generalizability of our approach.

Our automated pipeline, combining MRI measures of subcortical and cortical subregions, has comparable diagnostic accuracy to movement disorder neurologists in diagnosing early-stage PD and prodromal PD patients from HCs, at the single-subject level. This advance could reduce the burden on clinicians of vastly increasing numbers of PD patients and improve the power of trials investigating DMTs in PD.

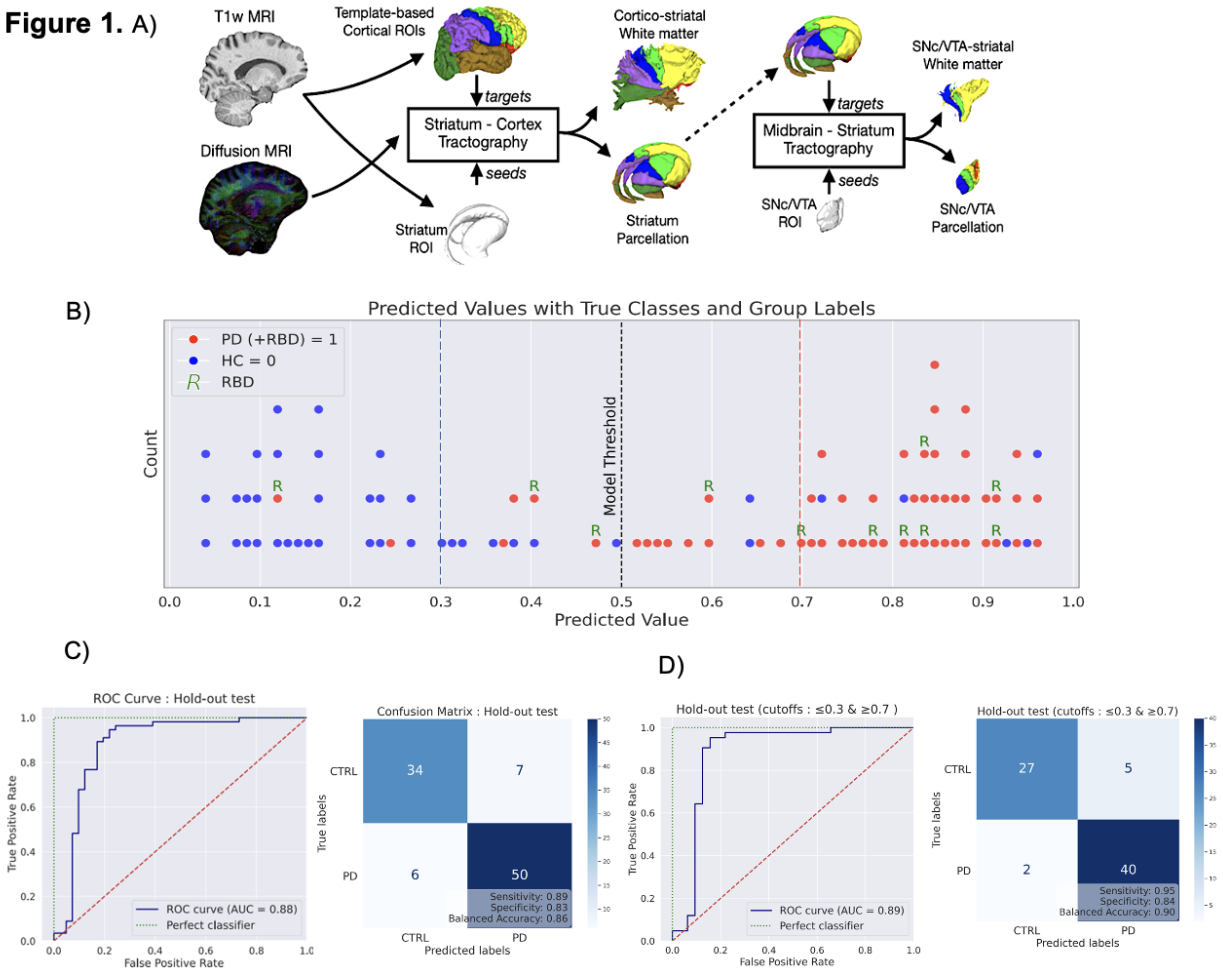

Figure 1. A) Schematic of connectivity-driven subject-specific parcellation of striatal and midbrain (SNc/VTA) sub-regions. ROIs defined by the CIT168 probabilistic subcortical atlas [1], are parcellated into sub-regions according to their tractography-based connection profiles to the cortex. These sub-cortical subregions are implicated in different functions [2] and each are affected distinctly by PD, which are important motives for considering them separately, B) Predicted values stratified by group with values above 0.5 identified as Parkinson's disease by the model, C) ROC curves and confusion matrices for the hold-out test set (n = 97) with subject-level categorizations of the model in the hold-out test set showing 50 true positives and 34 true negatives; sensitivity = 0.89, specificity = 0.83, and balanced accuracy = 0.86. When examining model performance at values ≤ 0.3 and ≥ 0.7, model performance is improved with sensitivity = 0.95, specificity = 0.84, and balanced accuracy = 0.90. This cut-off approach is more consistent with current clinical approaches which apply caution and re-evaluation in instances of greater uncertainty.

References

[1] Pauli WM, Nili AN, Tyszka JM. A high-resolution probabilistic in vivo atlas of human subcortical brain nuclei. Sci Data. 2018 Apr 17; 5: 180063. PMID: 29664465.

[2] Tziortzi AC, Haber SN, Searle GE, Tsoumpas C, Long CJ, Shotbolt P, Douaud G, Jbabdi S, Behrens TE, Rabiner EA, Jenkinson M, Gunn RN. Connectivity-based functional analysis of dopamine release in the striatum using diffusion-weighted MRI and positron emission tomography. Cereb Cortex. 2014 May; 24(5): 1165-77. PMID: 23283687.

LBA-16: Deep Brain Stimulation does not modify the cognitive trajectory of GBA-PD: a longitudinal study of the Italian PARKNET cohort

C. Artusi; R. Cilia; G. Giannini; G. Cuconato; C. Pasquini; A. Albanese; N. Andreasi; A. Antonini; L. Avanzino; A. Bentivoglio; F. Bove; M. Bozzali; G. Calandra-Buonaura; V. Carelli; F. Cavallieri; A. Cocco; F. Cogiamanian; F. Colucci; P. Cortelli; F. Di Biasio; A. Di Fonzo; V. D'Onofrio; R. Eleopra; A. Elia; V. Fioravanti; A. Guerra; C. Ledda; M. Liccari; C. Longo; L. Lopiano; M. Malaguti; F. Mameli; S. Marino; R. Minardi; E. Monfrini; C. Pacchetti; C. Piano; V. Rispoli; M. Rizzone; L. Romito; L. Sambati; M. Sensi; C. Sorbera; F. Spagnolo; C. Tassorelli; F. Valentino; F. Valzania; R. Zangaglia; M. Zibetti; The ParkNet Study Group; E. Valente (Italy)

Objective: To investigate the long-term motor, cognitive and non-motor outcome in GBA-PD after DBS treatment.

Background: GBA mutations occur in 10% of PD patients and are associated with worse non-motor outcome. Deep brain stimulation (DBS) is an established therapeutic option for PD, with significant improvement of motor symptoms also in GBA-PD patients. However, it remains unclear whether DBS may carry a higher risk of cognitive decline in GBA carriers, raising concerns on its indication in this frequent genetic PD subgroup.

Method: From the multicentric Italian PD PARKNET cohort, we selected 620 patients: i) 430 DBS-nonGBA-PD; ii) 113 DBS-GBA-PD; iii) 77 nonDBS-GBA-PD (patients who fulfilled CAPSIT-PD criteria for DBS but eventually were not operated). Detailed clinical info was collected at baseline (pre-DBS / time of CAPSIT-PD assessment) and after 1, 3 and, when possible, 5 years.

Results: At baseline, DBS-GBA-PD patients were younger and had earlier age at onset than other groups. Both operated and non-operated GBA-PD had a slightly lower disease duration that nonGBA-PD. The

three cohorts were fully comparable for motor, cognitive and other non-motor features, except for a higher prevalence of dyskinesias and orthostatic hypotension in DBS-GBA-PD and higher LEDD in the two groups who then underwent DBS. No differences were found in GBA-PD groups across class of variants in terms of mutation distributions and clinical features.

At longitudinal assessment, both DBS groups showed sustained motor improvement with significant control of fluctuations and LEDD decrease, a benefit which was absent in the nonDBS-GBA-PD cohort. Noteworthy, a more marked deterioration of cognitive scores was evident in both GBA groups compared to nonGBA-PD, regardless of DBS. Cognitive worsening in GBA carriers was already significant at 3-year and became more evident at 5-year follow-up, with no difference between DBS and non-DBS groups. No relevant differences were identified among carriers of different mutation types in both GBA-PD groups.

In the PARKNET GBA-PD cohort, DBS produced a relevant, sustained improvement of the motor phenotype, with no impact on the rate of cognitive decline. These data suggest that the higher rate of cognitive deterioration seen in mutated patients is part of the natural trajectory of GBA-PD and is not influenced by DBS, with major implications in the choice of the best therapeutic option for GBA-PD patients.

LBA-17: PSMF1 variants cause a phenotypic spectrum from early-onset Parkinson's disease to perinatal lethality by disrupting mitochondrial pathways

C. Tesson; P. Angelova; A. Salazar-Villacorta; J. Rodriguez; A. Scardamaglia; B. Chung; M. Jaconelli; B. Vona; N. Esteras; A. Kwong; T. Courtin; R. Maroofian; S. Alavi; R. Nirujogi; M. Severino; P. Lewis; S. Efthymiou; B. O'Callaghan; R. Buchert; L. Sofan; P. Lis; C. Pinon; G. Breedveld; M. Chui; D. Murphy; V. Pitz; M. Makarious; M. Cassar; B. Hassan; S. Iftikhar; C. Rocca; P. Bauer; M. Tinazzi; M. Svetel; B. Samanci; H. Hanağası; B. Bilgiç; J. Obeso; M. Kurtis; G. Cogan; A. Başak; G. Kiziltan; T. Gül; G. Yalçın-Cakmakli; B. Elibol; N. Barišić; E. Ng; S. Fan; T. Hershkovitz; K. Weiss; J. Raza Alvi; T. Sultan; I. Azmi Alkhawaja; T. Froukh; H. Abdollah E Alrukban; C. Fauth; U. Schatz; T. Zöggeler; M. Zech; K. Stals; V. Varghese; S. Gandhi; C. Blauwendraat; J. Hardy; S. Lesage; V. Bonifati; T. Haack; A. Bertoli-Avella; R. Steinfeld; D. Alessi; H. Steller; A. Brice; A. Abramov; K. Bhatia; H. Houlden (London, United Kingdom)

Objective: This study aims to dissect PSMF1 as new gene implicated in autosomal recessive early-onset Parkinson's disease/parkinsonism.

Background: Monogenic forms of Parkinson's disease (PD) and parkinsonism have unveiled crucial pathomechanisms that also underpin sporadic forms, highlighting a complex neurobiological network. Exploring biopathways highlighted by Mendelian gene discovery fosters the identification of biomarkers and development of disease-modifying strategies for PD, as exemplified with LRRK2 inhibitors.

Method: Genetics and variant functional characterization. Whole-exome or whole-genome sequencing were performed. PSMF1 variants identified were analyzed through pathogenicity prediction tools. Homozygosity mapping was performed for subjects carrying homozygous variants and their relatives. Haplotype analysis was performed in two probands beloging to different families and harboring the same homozygous variant. RNA sequencing or splicing assays were performed for splice variants.

Western blot of lysates from fibroblasts of one proband with a homozygous start-loss variant was performed.

Mitochondrial tests. Live cell imaging of cultured dermal fibroblasts for studying mitochondrial bioenergetic state and function was performed in cell donors from Pedigrees A-B-E-H-J-K (Figure 1). Images were acquired using Zeiss LSM 980 and LSM 710 confocal microscopes equipped with META detection system and 40× oil immersion objective. Images were analyzed using ZEN 2009 software and Fiji 2 software. For measurements of the mitochondrial membrane potential (ΔΨm), dermal fibroblasts were loaded for 40 minutes at room temperature with 25nM tetramethylrhodamine methylester (TMRM). We further studied the mitochondrial dynamics in the TMRM z-stacks by using the Mitochondrial Network Analysis (MiNA) toolset. To study mitophagy via mitochondrial and lysosomal co-localization, cells were loaded with 200nM MitoTracker Green FM and 50nM LysoTracker Red in HBSS for 30 minutes before experiments.

Drosophila modelling and behavioral tests. In D. melanogaster, we obtained targeted knockdown of psmf1 expression in conjunction with the UAS/Gal4/Gal80 system of cell-type-specific transgene expression by RNA-interference (RNAi). Transgenic RNAi flies were generated according to a previously published protocol. We crossed the RNAi lines psmf1, prkn and nsmase with an nSyb-Gal4 strain to drive pan-neuronal RNAi expression. Adult flies of the selected genotypes were tested for behavioral analyses at Days 10, 20 and 35. Based on previous studies and behavioral tests, prkn and nsmase were considered as positive and negative control, respectively. We assayed D. melanogaster locomotor activity using the climbing test based on negative-geotaxis analysis.

Mouse modelling, behavioral tests and neuropathology. Psmf1 knockout-first (KOF) mice were bred with a strain expressing FLP1 recombinase to generate a Psmf1 allele with the third exon flanked by 2 loxP sites (Psmf1fl and Psmf1tm1c(EUCOMM)Hmgu) as previously described. Rotarod and open field tests were used as behavioural assays. Immunofluorescence of mouse brain sections was performed.

Results: This study identifies PSMF1 as a new gene implicated in PD and early human neurodegeneration. By extensive data mining and functional validation, we establish that biallelic PSMF1 missense and loss-of-function variants cause a phenotypic spectrum ranging from early-onset PD to perinatal lethality with neurological manifestations, with clear genotype-phenotype correlation. We define the organellar and cellular consequences of PSMF1 deficiency in vitro through mitochondria live imaging of patient-derived cultured fibroblasts. Finally, we explore its pathological consequences in vivo in Drosophila and mouse models.

A total of 22 affected subjects from 15 unrelated families of European, Asian and African ancestry were identified. Genotype was determined for all but two individuals, who were included due to striking clinical resemblance to their affected siblings carrying homozygous PSMF1 variants in the context of parental consanguinity. The cohort comprised 11 males and 11 females. Parental consanguinity was reported in 9 of 15 pedigrees (60%). Probands' parents were healthy. Based on the phenotypic features and severity, we distinguished three subgroups across subjects with PSMF1-related disorder and recognized clear genotype-phenotype correlation (Figure 1).

In Pedigrees A-B-C-D-E-F-G, affected individuals manifested with early-onset PD or parkinsonism as the core phenotypic feature. In this subgroup, parkinsonism was most often accompanied by mild pyramidal tract signs, moderate-severe dysphagia occurring early in the disease course and psychiatric

manifestations. Brain MRI was normal or detected minor abnormalities, including mild-to-moderate cerebral or mild cerebellar atrophy. Four probands had markedly abnormal presynaptic dopaminergic imaging. Affected individuals had different degrees of response to dopaminergic treatments and tended to develop early motor and non-motor fluctuations and levodopa-induced dyskinesia. All affected individuals in this subgroup harbored PSMF1 missense variants, either in the homozygous state (Pedigrees B-C-D-E-F) or in compound heterozygosity with a predicted loss-of-function variant (Pedigrees A-G).

Affected individuals belonging to Pedigrees H-I-J-K presented with miscellaneous movement disorders, encompassing parkinsonism, moderate-to-severe pyramidal tract signs, ataxia or a combination thereof, most often in the context of neurodevelopmental delay and associated with mild-to-moderate intellectual disability, epilepsy and cognitive decline. They exhibited facial or skeletal dysmorphic features. In this subgroup, two probands had sensorineural hearing loss. Brain MRI almost invariably revealed hypoplasia of the corpus callosum and/or various degrees of cerebral or vermian cerebellar atrophy. Four patients died during adolescence because of rapidly progressive neurological deterioration starting early in the second decade of life. All affected individuals within this subgroup carried homozygous PSMF1 splice variants.

The third subgroup includes affected subjects from Pedigrees L-M-N-O, who presented with severe neurological manifestations since prenatal development, including arthrogryposis multiplex congenita, abnormal fetal movements (suspected for in utero seizures), epilepsy, profound developmental delay, limb spasticity, severe respiratory insufficiency and poor feeding, with death occurring within infancy. Agenesis or hypoplasia of the corpus callosum was detected in three probands. A history of pregnancy losses preceding the index case was reported in two of these pedigrees. All affected subjects in this subgroup had biallelic PSMF1 loss-of-function variants, of which at least one predicted to cause complete loss of function.

We detected 14 different PSMF1 mutant alleles, including five missense and nine loss-of-function variants (six splice, one nonsense, one start-loss and one frameshift; Figure 2). In all subjects with genomic DNA available, segregation analysis confirmed that biallelic PSMF1 variants co-segregated with neurological disease phenotypes. Moreover, parents of affected individuals harbored one heterozygous PSMF1 variant, and unaffected siblings of affected subjects were either heterozygotes for one PSMF1 mutant allele or homozygotes for the PSMF1 wild-type allele. Among 20 affected subjects with genotype available, 17 were homozygotes and 4 were compound heterozygotes for PSMF1 variants.

Fibroblasts from controls or PSMF1 carriers showed no effect or small increase in TMRM fluorescence after application of the mitochondrial complex V inhibitor oligomycin, indicating that that the enzyme is working as ATP synthase. On the contrary, addition of oligomycin to PSMF1 proband-derived fibroblasts induced >50% depolarization, which suggests that complex V is working in ATPase mode due to pathological mitochondrial electron transport chain functioning in these cells. Subsequent application of the inhibitor of mitochondrial complex I rotenone (5μM) induced decrease in TMRM fluorescence in control (by ~50%) or PSMF1 carriers' fibroblasts (by ~60%), whereas in PSMF1 probands' cells it induced complete mitochondrial depolarization, seen by the lack of effect of the mitochondrial uncoupler carbonyl cyanide p-trifluoromethoxyphenylhydrazone (FCCP; 1μM) on TMRM fluorescence after oligomycin and rotenone in these fibroblasts. In control or PSMF1 carriers' fibroblasts, subsequent application of FCCP induced further drop of the TMRM signal (by 30-40%) to a complete depolarization.

Mitochondria in PSMF1 proband- and control-derived fibroblasts differ not only by the TMRM signal intensity but also by their shape and size. Further analysis of the mitochondrial shape showed that mitochondria in the probands' fibroblasts appeared more fragmented and have shorter mitochondrial branch length and lower mean number of branches per network than control fibroblasts. We found that the percentage of co-localization in PSMF1 probands' fibroblasts was lower than in PSMF1 carriers. Mitophagy activation by 30mM lactate or 30mM pyruvate increased the percentage of mitochondria-lysosome co-localization in all fibroblasts, but to a higher extent in control and PSMF1 carriers' fibroblasts than in probands' fibroblasts.

In Drosophila melanogaster, we obtained pan-neuronal RNA interference (RNAi)-mediated targeted knockdown of psmf1. Motor performance was assessed using the classic negative-geotaxis climbing test and measured at different ages in psmf1 knockdown flies versus positive (prkn) and negative (nsmase) controls. At 10 and 20 days of age, we did not observe locomotor impairment in any of the three RNAi lines. In 35-day-old flies, motor performance was impaired in the psmf1 and prkn RNAi strains, with the mean proportion of flies which did not reach the 5-cm threshold being significantly lower compared to nsmase knockdown. Overall, these observations are consistent with Psmf1 loss of function causing age-dependent motor dysfunction in Drosophila.

In Psmf1 conditional knockout (CKO) mouse, we first assessed motor performances using the rotarod test. Psmf1fl/fl Ai14 UBC-429 Cre-ERT2 mice were injected with tamoxifen or corn oil as control at 6-7 weeks of age, while Psmf1fl/fl Ai14 mice without Cre were injected with tamoxifen as an additional control for tamoxifen. Ten days after the last injection, mice were trained for four days on the rotarod and then tested once on each day after for 11 days and thrice on the subsequent day. Initially the performance of tamoxifen-injected Psmf1fl/fl Ai14 Ubc-Cre-ERT2 mice with a high recombination rate (>90% of neurons as assessed by Ai14) displayed a deficit by day 12, whereas tamoxifen-injected Psmf1fl/fl Ai14 Ubc-Cre-ERT2 mice with a low recombination rate (approximately 30% of neurons as assessed by Ai14) showed only a mild deficit. Since individuals with PSMF1-related PD or parkinsonism present with severe anxiety, we also tested Psmf1fl/fl Ai14 UBC-Cre-ERT2 mice in the open field assay with dark insert. Anxiety-like behavior of rodents is frequently accompanied by reduced exploration. On day 26 after tamoxifen injection, Psmf1fl/fl Ai14 UBC-Cre-ERT2 mice displayed a clear difference to controls, consistent with increased anxiety. We observed gliosis in various brain regions 28 days after tamoxifen injection in Psmf1fl/fl Ai14 UBC-Cre-ERT2 mice. Many neurodegenerative diseases are associated with gliosis, where glial cells become reactive and proliferate generally prior to the formation of aggregates, tangles and plaques, including PD. Significantly, we detected both microgliosis, as documented by increased staining of microglia with anti-Iba1 and a change in morphology of the microglia from ramified to more amoeboid, and astrogliosis, as demonstrated by elevated GFAP-staining of astrocytes (Figure 3).

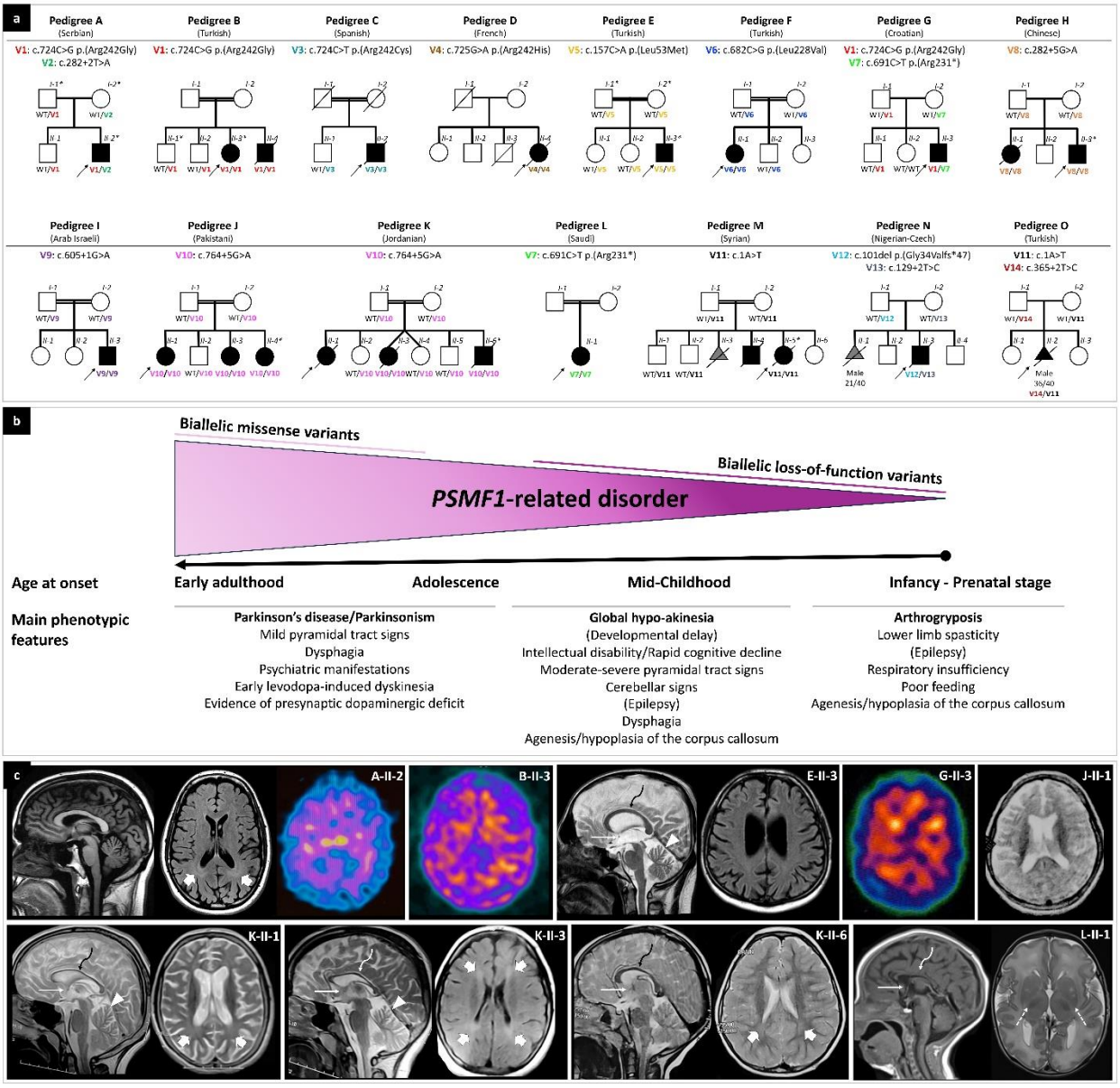
a
Pedigree A
(Serbian)
V1: c.724C>G p.(Arg242Gly)
V2: c.282+2T>A
Pedigree B
(Turkish)
V1: c.724C>G p.(Arg242Gly)
Pedigree C
(Spanish)
V3: c.724C>T p.(Arg242Cys)
Pedigree D
(French)
V4: c.725G>A p.(Arg242His)
Pedigree E
(Turkish)
V5: c.157C>A p.(Leu53Met)
Pedigree F
(Turkish)
V6: c.682C>G p.(Leu228Val)
Pedigree G
(Croatian)
V1: c.724C>G p.(Arg242Gly)
V7: c.691C>T p.(Arg231*)
Pedigree H
(Chinese)
V8: c.282+5G>A
Pedigree I
(Arab Israeli)
V9: c.605+1G>A
Pedigree J
(Pakistani)
V10: c.764+5G>A
Pedigree K
(Jordanian)
V10: c.764+5G>A
Pedigree L
(Saudi)
V7: c.691C>T p.(Arg231*)
Pedigree M
(Syrian)
V11: c.1A>T
Pedigree N
(Nigerian-Czech)
V12: c.101del p.(Gly34Valfs*47)
V13: c.129+2T>C
Pedigree O
(Turkish)
V11: c.1A>T
V14: c.365+2T>C
b
Biallelic missense variants
Biallelic loss-of-function variants
PSMF1-related disorder
Age at onset
Early adulthood
Adolescence
Mid-Childhood
Infancy - Prenatal stage
Main phenotypic features
Parkinson's disease/Parkinsonism
Mild pyramidal tract signs
Dysphagia
Psychiatric manifestations
Early levodopa-induced dyskinesia
Evidence of presynaptic dopaminergic deficit
Global hypo-akinesia
(Developmental delay)
Intellectual disability/Rapid cognitive decline
Moderate-severe pyramidal tract signs
Cerebellar signs
(Epilepsy)
Dysphagia
Agenesis/hypoplasia of the corpus callosum
Arthrogryposis
Lower limb spasticity
(Epilepsy)
Respiratory insufficiency
Poor feeding
Agenesis/hypoplasia of the corpus callosum
c
A-II-2
B-II-3
E-II-3
G-II-3
J-II-1
K-II-1
K-II-3
K-II-6
L-II-1

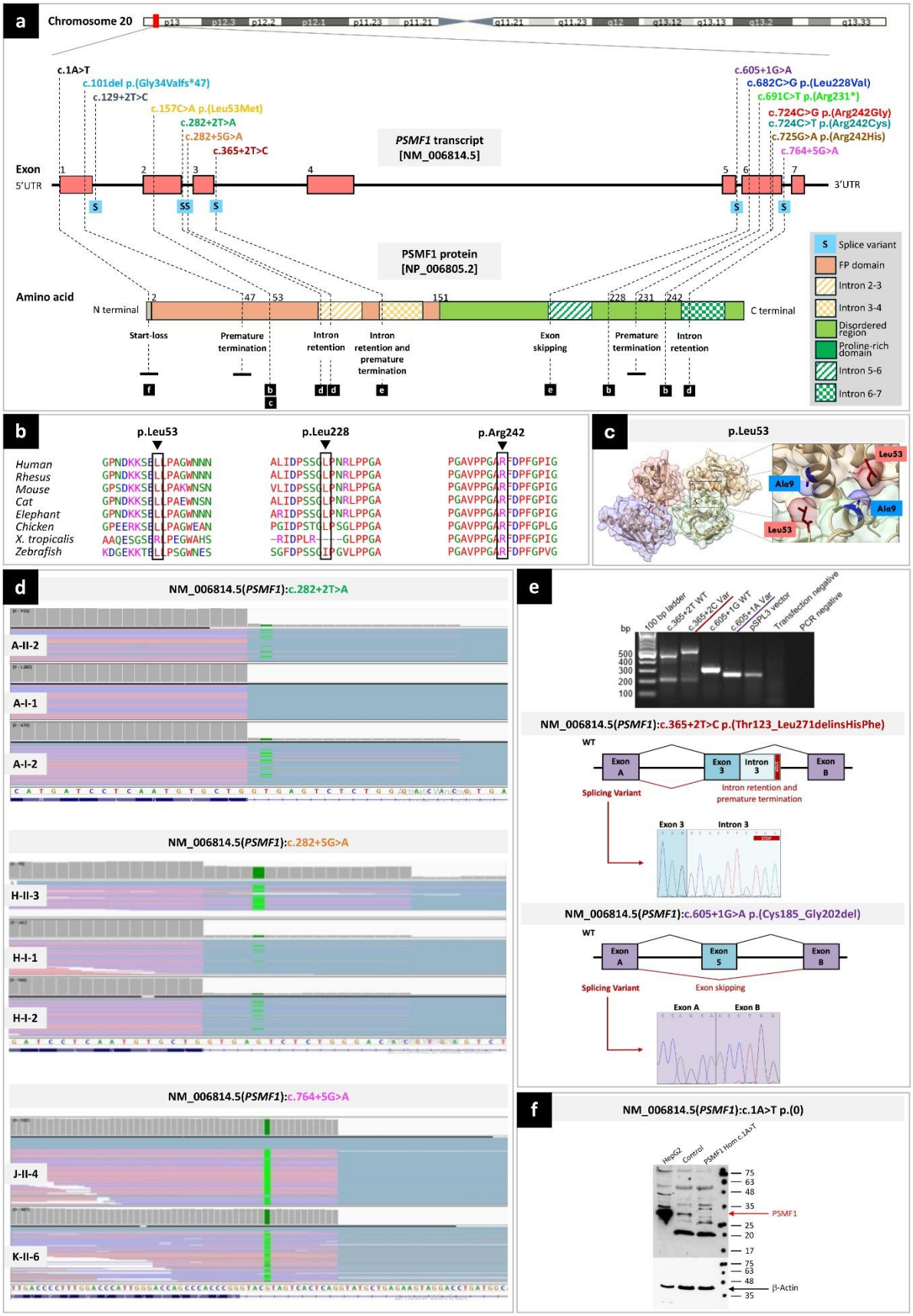
a
Chromosome 20
c.1A>T
c.101del p.(Gly34Valfs*47)
c.129+2T>C
c.157C>A p.(Leu53Met)
c.282+2T>A
c.282+5G>A
c.365+2T>C
c.605+1G>A
c.682C>G p.(Leu228Val)
c.691C>T p.(Arg231*)
c.724C>G p.(Arg242Gly)
c.724C>T p.(Arg242Cys)
c.725G>A p.(Arg242His)
c.764+5G>A
PSMF1 transcript [NM_006814.5]
Exon
5'UTR
3'UTR
PSMF1 protein [NP_006805.2]
Amino acid
N terminal
C terminal
Start-loss
Premature termination
Intron retention
Intron retention and premature termination
Exon skipping
Splice variant
FP domain
Intron 2-3
Intron 3-4
Disordered region
Proline-rich domain
Intron 5-6
Intron 6-7
b
p.Leu53
p.Leu228
p.Arg242
Human
Rhesus
Mouse
Cat
Elephant
Chicken
X. tropicalis
Zebrafish
c
p.Leu53
Leu53
Ala9
d
NM_006814.5(PSMF1):c.282+2T>A
A-II-2
A-I-1
A-I-2
NM_006814.5(PSMF1):c.282+5G>A
H-II-3
H-I-1
H-I-2
NM_006814.5(PSMF1):c.764+5G>A
J-II-4
K-II-6
e
100 bp ladder
c.365+2T WT
c.365+2C Var
c.605+1G WT
c.605+1A Var
pSPL3 vector
Transfection negative
PCR negative
bp
500
400
300
200
100
NM_006814.5(PSMF1):c.365+2T>C p.(Thr123_Leu271delinsHisPhe)
WT
Exon A
Exon 3
Intron 3
Exon B
Splicing Variant
Intron retention and premature termination
NM_006814.5(PSMF1):c.605+1G>A p.(Cys185_Gly202del)
Exon 5
Exon skipping
f
NM_006814.5(PSMF1):c.1A>T p.(0)
HepG2
Control
PSMF1 Hom c.1A>T
75
63
48
35
PSMF1
25
20
17
β-Actin

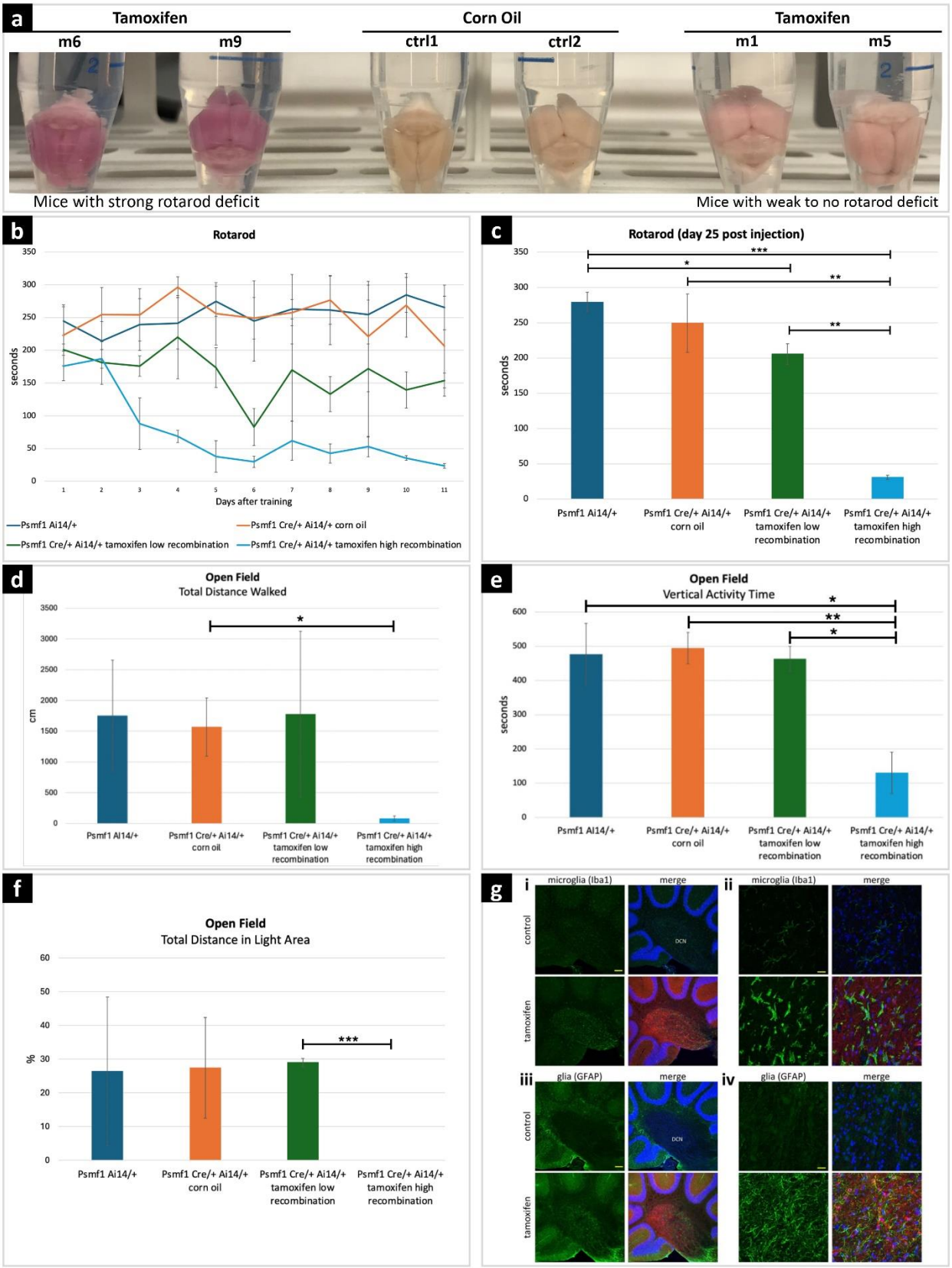
a
Tamoxifen
Corn Oil
Tamoxifen
m6
m9
ctrl1
ctrl2
m1
m5
Mice with strong rotarod deficit
Mice with weak to no rotarod deficit
b
Rotarod
seconds
Days after training
Psmf1 Ai14/+
Psmf1 Cre/+ Ai14/+ corn oil
Psmf1 Cre/+ Ai14/+ tamoxifen low recombination
Psmf1 Cre/+ Ai14/+ tamoxifen high recombination
c
Rotarod (day 25 post injection)
seconds
Psmf1 Ai14/+
Psmf1 Cre/+ Ai14/+ corn oil
Psmf1 Cre/+ Ai14/+ tamoxifen low recombination
Psmf1 Cre/+ Ai14/+ tamoxifen high recombination
d
Open Field
Total Distance Walked
cm
e
Open Field
Vertical Activity Time
seconds
f
Open Field
Total Distance in Light Area
%
g
microglia (Iba1)
merge
glia (GFAP)
control
tamoxifen
DCN

LBA-18: Preliminary Efficacy and Safety of ATH434 in Multiple System Atrophy

A. Brown; A. Wynn; C. Wong; K. Kmiecik; P. Trujillo; M. Bradbury; D. Stamler (Nashville, TN, USA)

Objective: To assess the efficacy, safety, and tolerability of ATH434 in participants with clinically established Multiple System Atrophy (MSA).

Background: MSA is a rapidly progressive neurodegenerative disorder that variably presents with parkinsonism, ataxia, and autonomic impairment. There are no approved disease modifying treatments. ATH434 is a moderate affinity iron chaperone which inhibits α synuclein aggregation, reduces oxidative stress and preserves neuronal function in an animal model of MSA. Here, we present interim data from an open label study of ATH434 in MSA participants.

Method: 10 participants with clinically established MSA, increased iron in the lentiform nucleus or substantia nigra (SN), and elevated plasma neurofilament light chain (NfL) received oral ATH434 75 mg bid for 12 months. 3T MRI and neurological exam were performed at 6-month intervals, including the Unified MSA Rating Scale part I (UMSARS I) clinical ratings. Patient- and clinical- global impressions of change (PGIC, CGIC) by 7-point Likert scale were assessed at 6- and 12-months. Biomarkers included iron content in SN by MRI QSM, brain volume by T1 weighted MRI (MSA-volume index), and CSF/plasma NfL levels at 6-month intervals.

Results: At the conference, we plan to report clinical, biomarker, and imaging data for 10 participants at baseline and 6-months, and 5 participants at 12 months of treatment. Interim analysis in 7 participants indicates that clinical response (stable or improved) was apparent in 2 participants based on UMSARS I and PGIC/CGIC scores. For N=7, the mean (SD) change in UMSARS I at 6 months was +1.7 (5.1). Brain volume declined in all participants between baseline and 6 months but stabilized in the clinical responders between 6 and 12 months. Stable iron content in the SN, putamen, and globus pallidus externa was seen in 3 participants. These results agreed with CSF NfL levels.

LBA-19: Results of ALLEVIA 1 (NOE-TTS-211; EudraCT 2021-004424-15; ANZCTR ACTRN12621000319875), a Phase 2a study exploring safety and tolerability of NOE-105 in patients with Tourette Syndrome

G. Garibaldi; R. Lasser; K. Mueller-Vahl (Hannover, Germany)

Objective: To explore the safety and tolerability of NOE-105, a unique and potent PDE10A inhibitor, as well as its ability to alleviate tics in Tourette Syndrome (TS) to support development planning in TS.

Background: TS is characterized by the presence of motor and vocal tics for more than 1 year with childhood onset. It is present in about 1 out of 160 children and adolescents in the US. Comorbidities include attention deficit/hyperactivity disorder (ADHD), obsessive-compulsive disorder (OCD), depression, anxiety, and autism spectrum disorders. Tics may highly impact the social, academic, and professional life of patients. Current therapies consist of behavioral therapy and alpha-adrenergic agents or antipsychotic drugs that are often associated with adverse events (AEs) such as sedation and weight gain.

Method: NOE-TTS-211 was an open label, international, multicenter study, enrolling 15 adults and adolescents. After consent and discontinuation of previous TS medication, participants were treated with daily doses of 2.5 to 15 mg over the 12-week treatment period, including titration and maintenance. Safety was assessed by AE monitoring, labs analyses, ECG, and other safety scales. The primary efficacy endpoint was the adjudicated Clinical Global Impression of Change (CGI-C), executed by a Response Assessment Committee chaired by an independent TS expert. Secondary endpoints included the Yale Global Tic Severity Scale (YGTSS), clinician and patient measures of global change, and the ADHD rating scale (ADHD-RS-IV).

Results: A total of 15 patients (13 adults, 2 adolescents) were enrolled in the study. The summary of the study results will be added by the 15 Aug 2024.

LBA-20: Nonhuman primate efficacy and safety of snp614, a lrrk2 antisense oligonucleotide as potential therapeutic agent for parkinson's disease

A. Zembrzycki;Y. Martens; I. Riera Tur;S. Michel; R. Klar; F. Jaschinski; G. Bu; M. Li (Rockville, MD, USA)

Objective: To develop therapeutic agents capable of reducing LRRK2 mRNA to lower PD-associated LRRK2 overactivation in the central nervous system (CNS).

Background: Parkinson's disease (PD) is a progressive neurodegenerative disorder characterized by the degeneration of dopaminergic neurons in the substantia nigra and a deficiency of dopamine in the striatum. Pathogenic mutations in the Leucine-Rich Repeat Kinase 2 (LRRK2) gene are strong genetic risk factors for PD. Majority of disease-associated LRRK2 mutations appear to be toxic; most notably, some lead to increased LRRK2 kinase activity that disrupts multiple aspects of normal cellular physiology. Previously, we have reported the discovery effort of SNP614, the leading ASO candidate against LRRK2. Here, we report in vivo efficacy and safety of SNP614 in both rodents and nonhuman primates (NHPs).

Method: SNP614 was administered to rodents and NHPs via intracerebroventricular or intrathecal delivery. The drug distribution in the CNS, pharmacokinetics, activities, and preliminary safety assessments of SNP614 in NHP were investigated.

Results: SNP614 has exhibited broad distribution and long-lasting knock-down effect including significant LRRK2 reduction in deep brain regions critical for achieving PD treatments. It exhibits excellent target engagement (TE), in vitro/in vivo (IVIV), and pharmacokinetic/pharmacodynamic (PK/PD) correlation, as well as long-lasting and exposure dependent efficacy and safety.

We report the discovery of SNP614, the lead development candidate, that reduces LRRK2 mRNA levels to broadly lower PD-associated LRRK2 overactivation in NHP CNS. It is potent, efficacious, and well-tolerated, and has excellent potential to be developed as therapeutic agents to slow the PD pathology and disease progression.